

**Numerical computations of the unsteady flow in  
a radial turbine.**

by

Fredrik Hellström

March 2008  
Technical Reports from  
Royal Institute of Technology  
KTH Mechanics  
SE-100 44 Stockholm, Sweden

Akademisk avhandling som med tillstånd av Kungliga Tekniska Högskolan i Stockholm framlägges till offentlig granskning för avläggande av teknologie licentiatexamen fredagen den 28 mars 2008 kl 13.00 i sal E3, Osquarsbacke 14, Kungliga Tekniska Högskolan, Vallhallavägen 79, Stockholm.

©Fredrik Hellström 2008  
Universitetsservice US-AB, Stockholm 2008

# Numerical computations of the unsteady flow in a radial turbine.

**Fredrik Hellström 2008,**

KTH Mechanics

SE-100 44 Stockholm, Sweden

## Abstract

Non-pulsatile and pulsatile flow in bent pipes and radial turbine has been assessed with numerical simulations. The flow field in a single bent pipe has been computed with different turbulence modelling approaches. A comparison with measured data shows that Implicit Large Eddy Simulation (ILES) gives the best agreement in terms of mean flow quantities. All computations with the different turbulence models qualitatively capture the so called Dean vortices. The Dean vortices are a pair of counter-rotating vortices that are created in the bend, due to inertial effects in combination with a radial pressure gradient. The pulsatile flow in a double bent pipe has also been considered. In the first bend, the Dean vortices are formed and in the second bend a swirling motion is created, which will together with the Dean vortices create a complex flow field downstream of the second bend. The strength of these structures will vary with the amplitude of the axial flow. For pulsatile flow, a phase shift between the velocity and the pressure occurs and the phase shift is not constant during the pulse depending on the balance between the different terms in the Navier-Stokes equations.

The performance of a radial turbocharger turbine working under both non-pulsatile and pulsatile flow conditions has also been investigated by using ILES. To assess the effect of pulsatile inflow conditions on the turbine performance, three different cases have been considered with different frequencies and amplitude of the mass flow pulse and different rotational speeds of the turbine wheel. The results show that the turbine cannot be treated as being quasi-stationary; for example, the shaft power varies with varying frequency of the pulses for the same amplitude of mass flow. The pulsatile flow also implies that the incidence angle of the flow into the turbine wheel varies during the pulse. For the worst case, the relative incidence angle varies from approximately  $-80^\circ$  to  $+60^\circ$ . A phase shift between the pressure and the mass flow at the inlet and the shaft torque also occurs. This phase shift increases with increasing frequency, which affects the accuracy of the results from 1-D models based on turbine maps measured under non-pulsatile conditions.

For a turbocharger working under internal combustion engine conditions, the flow into the turbine is pulsatile and there are also unsteady secondary flow components, depending on the geometry of the exhaust manifold situated upstream of the turbine. Therefore, the effects of different perturbations at

the inflow conditions on the turbine performance have been assessed. For the different cases both turbulent fluctuations and different secondary flow structures are added to the inlet velocity. The results show that a non-disturbed inlet flow gives the best performance, while an inflow condition with a certain large scale eddy in combination with turbulence has the largest negative effect on the shaft power output.

**Descriptors:** Pulsatile flow, radial turbines, pipe flow, effects of inlet conditions, Large Eddy Simulation.

## Preface

This licentiate thesis in fluid mechanics consist of two parts. The first part gives an overview of the research area and a summary of the results. The second part consists of 3 papers, which are adjusted to comply with the present thesis format for consistency. However, their contents have not been changed compared to published or submitted versions except for minor refinements. In Chapter 7 of the first part of the thesis the respondent's contribution to all papers are stated.

March 2008, Stockholm

*Fredrik Hellström*



# Contents

<b>Abstract</b>	iii
<b>Preface</b>	v
<b>Chapter 1. Introduction</b>	1
<b>Chapter 2. Non-pulsatile and pulsatile internal flow</b>	3
2.1. Flow in curved pipes	3
2.2. Internal pulsatile flow	5
<b>Chapter 3. Turbochargers, with focus on the turbine</b>	9
3.1. Performance parameters	9
3.2. The stator	11
3.3. The rotor	16
3.4. Turbine performance under pulsatile flow	19
<b>Chapter 4. Methods</b>	25
4.1. Governing equations	25
4.2. Turbulence	26
4.3. Numerical methods	27
4.4. Numerical accuracy and uncertainty	32
4.5. Comparison of computed and measured data	34
<b>Chapter 5. Results</b>	36
5.1. Non-pulsatile and pulsatile flow in curved pipes	36
5.2. Unsteady flow in a radial turbine	42
<b>Chapter 6. Conclusions</b>	56
6.1. Future work	57
<b>Chapter 7. Papers and authors contributions</b>	59

<b>Acknowledgements</b>	62
<b>References</b>	63
<b>Paper 1</b>	73
<b>Paper 2</b>	93
<b>Paper 3</b>	117

# Part I

## Overview and summary



## CHAPTER 1

### Introduction

A turbine is a flow device that extracts energy from a fluid by expanding it through a stator and rotor system and when the fluid passes the rotor with a high tangential velocity, it causes the rotor to rotate. The fluid can be a gas or a liquid depending on the applications. The turbine can be either a radial or an axial turbine. In axial turbines, the main flow direction at the inlet to the rotor is parallel to the turbine shaft while for radial turbines, the main flow direction at the inlet to the rotor is perpendicular to the shaft. Axial turbines can be found in gas turbines, which are used for example for aircraft propulsion, power generation and ship propulsion. In a gas turbine, the working gas of the turbine is the exhaust gas from combustion chambers situated upstream of the turbine. The turbine, which may consist of several turbine stages, is used to drive the compressor stages, which are used to increase the amount of air to the combustion chamber. The turbine can also drive a generator when it is used for power generation and propulsion systems on ships. Axial turbines are also used in power plants, and the working gas in this application can be steam, produced by a boiling process with different types of heat sources. In this application, the turbine drives a generator. Another area where turbines are used is in hydroelectric power plants, where the working fluid is water. Often one uses also in this area radial (i.e. Francis) turbines. Radial turbines are also used in the aerospace area, where they are used for driving fuel pumps.

The area where radial turbines are used in largest numbers is probably in the turbocharger application for Internal Combustion (IC) engines. In a turbocharger, the energy of the engine exhaust gas is extracted by expanding it through the turbine which drives the compressor by a shaft. This means that the wasted energy in the exhaust gas, which can be roughly 30-40 percent of the chemical energy released by the combustion, is used to increase the density of the air admitted to the cylinder. Thereby the power output of the engine can be increased or alternatively the engine size can be reduced, without decreasing the power output. If a turbocharged IC engine is compared with a natural aspirated engine with the same power output, the turbocharged engine will be smaller, lighter and requires a smaller installation space. The turbocharged IC engine will also have a better efficiency, since the inertia of system is less

and the friction losses are decreased due to smaller cylinders, valves etc. This technique is called downsizing and can be used to meet the future demands on lower fuel consumption and emission levels with maintained, or even increased, power output. To be able to further increase the efficiency of the IC engine, the understanding of the highly pulsatile flow in the turbine part of the turbocharger must be improved. This knowledge will also be used to increase the efficiency of the turbine and also to develop a low order numerical model of the turbine to be used in numerical engine simulation tools. In this thesis, the performance of the turbine working in both non-pulsatile and pulsatile flows is considered.

The main focus of the work has been on:

- The physics of pulsatile flow in bent pipes.
- Assessment of the effects of inflow conditions on the turbine performance.

For the later case, both the effects of pulsatile and non-pulsatile flow have been assessed, with varying perturbations and unsteadiness applied at the inlet to the turbine. The used method is time resolved three-dimensional numerical simulations.

The work described in the thesis mark a contribution in understanding the flow in the turbine and its dependence on the inflow conditions. The latter aspect is of importance from engineering point of view; i.e. for the integration of the turbo-charger in the car engine. By improved understanding of the flow, a better understanding the sources of losses in the turbine is achieved. The experience gained in the computational analysis shall hopefully help in improving the modelling of such flows.

The remainder of the thesis is organized as follows: In Chapter 2 a brief overview of the steady and unsteady flow in pipes is given. This chapter is followed by Chapter 3 where the features of turbochargers, with focus on the turbine part, are discussed. Chapter 4 consider the used methods. In Chapter 5, the most important results are presented followed by conclusions in Chapter 6. Finally, in Chapter 7, a short summary of the included papers is given.

## CHAPTER 2

### Non-pulsatile and pulsatile internal flow

The purpose of this chapter is to give a brief overview of the pulsatile internal flow in pipes since the flow in an exhaust system on an IC engine is highly pulsatile. The exhaust manifold, situated between the engine and the turbine, can be viewed as being made of straight and curved pipe sections. Therefore, the flow in bent pipe has also been considered. The frequency and the amplitude of the pulsatile flow in the exhaust system will be determined by the numbers of cylinders of the engine and at which operation point the engine is working, i.e. the engine rotational speed and the throttle position. The geometry of the exhaust manifold will also affect the flow into the turbine, since single and double bends will introduce secondary flow, junctions will disturb the flow and there are also pressure waves that will be reflected in the manifold. Therefore, a literature survey on the steady and unsteady flow in different pipe configurations has been conducted.

#### 2.1. Flow in curved pipes

There are many applications where flow in bent pipes can be found, for example pipe-lines, exhaust systems and the blood flow in arteries. One typical feature of the flow in bent pipes is the so called Dean vortices, which are a pair of counter-rotating vortices. When the flow enters the bend, the fluid is accelerated near the inner wall. Simultaneously, the fluid near the outer wall is decelerated due to the adverse pressure gradient. This induces a secondary flow in the transverse plane of the pipe. Further downstream, the centrifugal force induces a second flow in the central part of the cross section from the inner wall to the outer wall and forms the two counter-rotating vortices, see Figure 2.1.

Sudo *et al.* (1998) investigated the steady turbulent flow in a circular-sectioned  $90^\circ$  bend. The curvature radius ratio, defined as the ratio between the radius of the bend and the pipe radius, was four and the flow was assumed to be turbulent. At the inlet to the bend,  $\varphi=0^\circ$ , the primary flow accelerates near the inner wall. At  $\varphi=30^\circ$  the secondary flow starts to develop into a counter rotating pair of vortices. Between  $\varphi=75^\circ$  and  $90^\circ$  the primary flow is greatly distorted and the turbulence intensity and Reynolds stresses increases. Downstream of the bend, the distribution of primary flow velocity gradually

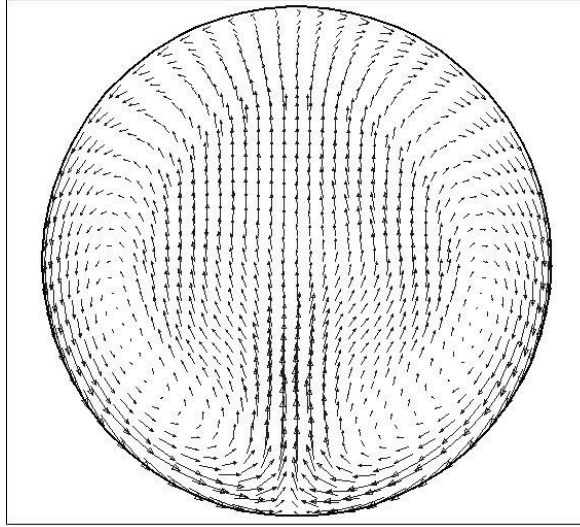


FIGURE 2.1. The counter-rotating Dean vortices.

becomes smooth and the vortices break down, but the effect of secondary flow remains at 10 diameters downstream of the bend. Sudo & Hibara (2000) also performed measurements on a  $180^\circ$  bend. The curvature radius was the same as for the  $90^\circ$  bend. Upstream to  $\varphi=60^\circ$  the flow in the two different geometries shows similar characteristics. From  $\varphi=90^\circ$  the secondary flow begins to weaken and meanders up and down in the central part of the tube. In this part of the bend, a low-velocity region exists in the middle and high velocity regions are located near the inner and outer walls.

Rutten *et al.* (2005) performed Large Eddy Simulations to investigate the turbulent flow through  $90^\circ$  pipe bend. The purpose of this investigation was to see how long the extension must be to avoid distortion of the flow field from the bend at the inlet boundary. The conclusion from the investigation was that an extension length of three diameters is sufficient. The computed data is validated by comparing the first and second order statistical moments with PIV measurements by Brucker (1998). Power spectra of LES and PIV velocity signals are also compared and the agreement of the numerical and experimental results is good. The computed flow field showed the counter-rotating Dean vortices, which are not of equal strength at all times and alternately dominate the flow field. This alternately domination leads to alternately clockwise and anti-clockwise rotation of the flow close to the wall in the downstream tangent.

If a pipe is turned in two bends, with the bends in orthogonal planes, a swirling motion will be generated after the second bend, as seen Figure 2.2. The

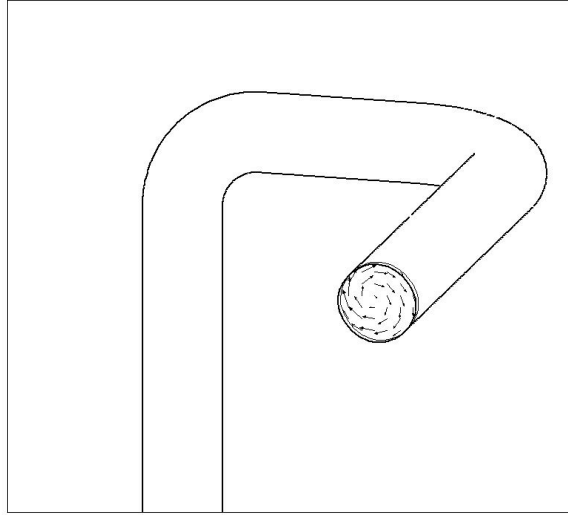


FIGURE 2.2. The swirl at the outlet of a double bent pipe.

swirling motion at the outlet of the second bend is not an effect of the Dean vortices from the first bend; it is an effect of the non-uniform axial velocity distribution in radial direction at the inlet to second bend. If a non-uniform radial velocity distribution, with the maximal value rotated  $90^\circ$  with respect to the inner radius of the bend, is applied to the inlet to a single bend, the secondary flow consist of one vortex at the outlet of the bend. When the flow with high velocity and momentum enters the bend it is linked by the curvature to the region where the momentum is lower which induces a swirling motion. Since very few articles were found for this geometry, a numerical investigation of the pulsatile flow in a double bent pipe was performed, and the results are discussed in Chapter 5.

## 2.2. Internal pulsatile flow

An oscillating flow, which is a special type of pulsatile flow, only consists of the time varying component, and hence the periodically time-averaged velocity is zero. Pulsatile flow is defined here as a flow that is composed of a steady component with a superimposed periodically varying temporal component. The behaviour of oscillating or pulsatile flow depends on the balance between the viscous effect and the acceleration of the fluid. The relative importance of the acceleration term relative to the viscous term in the momentum equation can be expressed by the Womersley number, defined as:

$$\alpha = r \cdot \sqrt{\frac{2\pi \cdot f}{\nu}} \quad (2.1)$$

where  $r$  is the pipe radius,  $f$  the frequency and  $\nu$  is the kinematic viscosity. A small value of the Womersley number implies that the effects of unsteadiness are less important as compared to viscous effects. For low Womersley number ( $\alpha < 1$ ), the velocity is nearly a quasi-steady Poiseuille flow which is in phase with the pressure gradient. As the Womersley number increases, the velocity starts to show a phase lag with respect to the pressure gradient. For all pulsating flows, a phase shift between the axial flow and the pressure gradient occurs, see for example Dec *et al.* (1991) and Ramaprian & Tu (1983). For pure oscillating very low Reynolds number flow the phase lag is  $90^\circ$  and for turbulent flow the phase lag is less than  $90^\circ$  according to Ramaprian & Tu (1983). For pure oscillating very low Reynolds number flow, the  $\frac{\partial}{\partial t}$ -term in the momentum equation (4.2) is balanced by the  $\frac{\partial p}{\partial x_i}$ -term. This can be showed by assuming one-dimensional oscillating flow and that the pressure gradient is described by  $\frac{\partial p}{\partial x} = \hat{p} \cdot e^{i\omega t}$  where  $\hat{p}$  is a constant and  $\omega$  is the frequency of the oscillation. When this is inserted into the momentum equation (4.2) and solved for  $U$ , the following result is obtained  $U = -\frac{i\hat{p}}{\omega} \cdot e^{i\omega t}$ . As can be seen, the phase shift between the velocity and the pressure is  $90^\circ$ . For pulsatile turbulent flow, the time derivate term will be balanced both by the pressure gradient term and remaining terms in the momentum equations, including the Reynolds-stresses. Flow pulsations also affect the axial velocity profile in the pipe. The phase shift between the pressure and the bulk velocity gives overshoots in boundary layer which depends on that the flow in the region near the wall has lower momentum than the bulk flow, and therefore, it is more sensitive to changes in the axial pressure gradient. This effect increases with increasing frequency due to the inertia effect. Ramaprian & Tu (1983) carried out an experimental study of turbulent oscillatory flow in a long circular pipe. The oscillating frequencies correspond to a Womersley number of approximately 43 and 116, respectively. They compared the results with theoretical results for laminar oscillating pipe flow at the same frequency. The laminar flow shows sharper peaks of the overshoots in the boundary layer than the turbulent flow. Also, the peaks occur closer to wall for the theoretical laminar case. The experiments also show that the phase lag between pressure and velocity is smaller for turbulent flow than for the laminar flow. Dec *et al.* (1991) investigated a cyclic oscillating velocity field in a tail pipe of a pulse combustor using Laser Doppler Velocimetry (LDV). The oscillating frequencies varied from 67 to 101 Hz and the amplitude was up to 5 times the mean velocity. The mean Reynolds number was 3750. The turbulent flow shows a similar behaviour to the theoretical laminar oscillating pipe flow, with a phase shift between the pressure and the velocity and an overshoot near the wall. The flow near the wall reverses earlier than

the flow in the core region. The laminar flow solution also shows a sharper overshoot relative to the core region profile, while the turbulent flow has a smoother axial velocity profile. The reason is, according to Dec *et al.* (1991), that in turbulent flow the additional momentum transport by the turbulence rapidly dissipates the oscillations. The turbulence intensity is uniform across the core region of the flow, but the behaviour in the boundary layer has two different modes. When the streamwise pressure gradient is adverse, the turbulent intensity increases from the core to a maximum in the boundary layer and then going to zero at the wall. When the pressure gradient is favourable, the turbulent intensity drops from the core value throughout the boundary layer. The turbulent intensity also shows a maximum at times of zero-velocity crossings. From the measured velocity profiles, the instantaneous wall shear stresses were calculated. A trend of increasing cycle-averaged wall shear stress with increasing pulsation amplitude can be noted but no dependence on the frequency was found. The cycle-averaged wall shear stress is slightly greater than the wall shear stress predicted for steady turbulent flow at the same averaged mean Reynolds number.

For laminar pulsating flow in a bent pipe, the secondary flow changes rotational direction from being outward to inward in the centre when Reynolds number is increased for a certain Womersley number. Hamakiotes & Berger (1988) showed using numerical computations, that the Dean vortices do change rotation direction when Re exceeds 300. The Womersley number was 15 and curvature ratio was 1/7. The reversed vortices are called the Lyne vortices. Lyne (1970) showed analytically that the fluid is driven along the wall from the outer side to inner side under action of the pressure gradient in the same manner as for the Dean vortices. However, the pressure gradient in the boundary layer is not balanced by the centrifugal forces, and at the edge of the boundary layer, the flow returns centrifugally within in the boundary layer, and drags the fluid in the interior around in a pair of vortices, that are counter-rotating compared to the Dean vortex.

It may be expected that the heat transfer to or from a flow in a pipe should depend on the pulsation frequency, since the pulsations will affect the boundary layer. Both increase and decrease of the Nusselt number in pulsating flow has been reported in the literature for different pulsation frequencies, amplitudes and mean Reynolds numbers. The Nusselt number is defined as the ratio between the convective and conductive heat transfer:

$$Nu_L = \frac{h_{coef} \cdot L}{k_f} \quad (2.2)$$

$h_{coef}$  is the heat-transfer coefficient,  $L$  is a characteristic length scale and  $k_f$  is the thermal conductivity. Wang & Zhang (2005) performed numerical computations of turbulent pulsatile flow in a straight pipe with  $U_{osc}/U_{mean}=3$ ,

where the Womersley number was varied from 40 to 60. The results showed that the axial pressure gradient has a phase lag of about  $90^\circ$  to the velocity. The results also showed that the instantaneous velocity profile was flat at the centre of the pipe. In the region between the core region and the wall a velocity overshoot occurred at some instants. These overshoots had a velocity that was larger than the velocity in the core region, and more heat was transported at these instances. The thermal boundary layer thickness varied with the pulsation of the flow and was during a period, sometimes thinner and sometimes thicker than in a corresponding steady state flow case. The local Nusselt number was, for different Womersley numbers, higher than it was for the corresponding steady case. The heat transfer was greatly enhanced by the pulsative flow, especially in the entrance region. Wang and Zhang also showed that the local instantaneous Nusselt number had its maximum when the velocity reached its peak value and the Nusselt number reached its lowest value when the velocity was zero. The heat transfer was also enhanced when the velocity amplitude of the pulse was increased. The results from Dec & Keller (1989) experiments with a pulse combustor fitted with a tail-pipe showed that the Nusselt number in oscillating flow was significantly higher than for steady flow with the same mean Reynolds number. The experiments also showed that the Nusselt number increased with increasing frequency and pulsation amplitude. Habib *et al.* (2004) studied pulsatile pipe flow in a range of  $Re$  of  $8\,000 < Re < 50\,000$  and both enhancement and reduction in mean Nusselt number was reported. The Nusselt number decreased for low pulsating frequency. The maximum mean Nusselt number was obtained when the pulsating frequency was in the vicinity of the turbulent bursting frequency. At this pulsating frequency, the interaction of the pulsations and the turbulent bursting increased the heat transfer, and hence the Nusselt number increased. These phenomena can be explained by the turbulent bursting model, which states that the viscous sublayer is unstable, and due to turbulent structures, its growth and destruction occur periodically.

These different effects, such as the phase lag and increased heat transfer in pulsatile flow, will affect the performance of the radial turbine working under pulsatile flow conditions. The phase shift will imply that the static and dynamic pressure will be out of phase, which can affect the shaft power of the turbine. The pulsatile flow also increases the losses; for example the heat-losses to the ambient. The losses due to viscous effects will probably also increase, due stronger shear layers. This will most probably imply that the turbine cannot be treated as being a quasi-stationary flow device.

## CHAPTER 3

### Turbochargers, with focus on the turbine

Turbochargers can be used in many different applications, but they are all based on the same principle. A turbocharger has four principal components, a compressor, a turbine, a shaft and bearings. The turbine part utilizes the energy from the hot gas that flows through the turbine and drives a compressor which will increase the density of the gas. The bearings support the shaft, and shaft seals are also required to separate the compressed air and the exhaust gases from the bearing lubrication system. Turbochargers can be found on different types of internal combustion (IC) engines, from small four-stroke automotive engines to large two-stroke marine diesel engines. For small internal combustion engines, radial turbines are the most common type. Axial turbines are used for large IC engines in marine and power generation applications. The rotational speed of the turbine is normally limited by the requirements of the compressor and the maximum radius for a given rotational speed is limited by structural reasons. This means, for turbines that normally are used for small IC engines, that the radius of the turbine wheel must be small. For small axial turbines, this gives an unfavourable aspect ratio which will give rise to secondary flows and tip leakages which will result in poor efficiency. Since axial turbines also are complicated and more expensive compared with radial turbines, the most common type of turbines for small IC engines is the radial type. Radial turbines can also deliver a larger specific power than an equivalent axial turbine. For small engines, like those used for passenger car, the pressure ratio over the compressor is about 2 and the speed can range up to about 300 000 rpm.

#### 3.1. Performance parameters

The fundamental parameters for turbines that define the performance are the mass flow, the pressure ratio, the rotational speed, the efficiency and the power output. The most important quantity for the turbine is the shaft power,  $P_S$ , which is defined here as

$$P_S = \bar{T}_{Shaft} \cdot \bar{\omega} \quad (3.1)$$

where  $\bar{\omega}$  is the angular velocity and  $\bar{T}_{Shaft}$  is the shaft torque. In the computations, the shaft torque is obtained by integrating the element forces due to the shear and pressure forces times the radial coordinate over the turbine wheel:

$$\bar{T}_{Shaft} = \int_S \bar{r} \times (\bar{f} \cdot \hat{n}) dS \quad (3.2)$$

Another important quantity is the turbine efficiency,  $\eta_{is}$ . Commonly one defines the efficiency as the ratio of shaft power to the maximal isentropic power of the driving gas flow:

$$\eta_{is} = \frac{P_S}{\dot{m} \cdot c_p \cdot T_{01} \cdot \left(1 - \frac{p_2}{p_{01}}\right)^{\frac{\gamma-1}{\gamma}}} \quad (3.3)$$

where  $\dot{m}$  is the mass flow,  $T_{01}$  and  $p_{01}$  is the total gas temperature and pressure before the turbine and  $p_2$  is the static pressure downstream of the turbine.  $c_p$  is the specific heat and  $\gamma$  is the specific heat ratio. This definition works well for non-pulsatile flow and for pulsatile flow at moderate frequencies. For higher frequencies, the non-constant phase shift between the mass flow, pressure and shaft torque makes it impossible to define an isentropic efficiency in a proper way.

The fundamental parameters can either be predicted by using analytic or semi-analytic models or by testing the turbocharger under controlled conditions. The fundamental parameters are often non-dimensionalized, see Table 1, to take account for the inlet conditions and are often reported in compressor and turbine maps. Since the diameter,  $D$  for a particular turbine is constant, it can be dropped. The turbines are also tested with the actual working gas, and hence, the gas constant  $R$  and  $\gamma$  can also be dropped. By doing so, the quasi-non dimensional parameters are obtained. The performance can also be reported as the referred parameters, which have the same units as the fundamental parameters. In the referred parameters, the inlet pressure and temperature are referred to reference values.

The performance of a turbine is tested in gas stand where the turbine is driven by gas from an external compressor. The measurement can be performed both with cold and hot gas. In the later case, fuel is injected and burnt in a combustion chamber upstream of the turbine. Since the rotational speed is very high, it is very hard to directly measure the shaft power output of the turbine. Therefore, the compressor is throttled to control the load on the turbine, and by measuring the shaft speed, the inlet and outlet pressure, temperature and the mass flow through the turbine and the compressor, respectively, the efficiency of the turbine can be computed. This efficiency is the mechanical efficiency, since the bearing losses are included. The mechanical efficiency can be divided into

TABLE 1. Dimensional and non-dimensional parameters as defined by Baines (2005).

	Fundamental parameters	Non dimensional parameters	Quasi-non dimensional parameters	Referred parameters
Mass flow	$\dot{m}$	$\frac{m\sqrt{RT_0/\gamma}}{p_0 D^2}$	$\frac{m\sqrt{T_0}}{p_0}$	$\frac{m\sqrt{T_0/T_{ref}}}{p_0/p_{ref}}$
Pressure ratio	$PR$	$PR$	$PR$	$PR$
Rot. speed	$N$	$\frac{N \cdot D}{\sqrt{\gamma \cdot R \cdot T_0}}$	$\frac{N}{\sqrt{T_0}}$	$\frac{N}{\sqrt{T_0/T_{ref}}}$
Efficiency	$\eta$	$\eta$	$\eta$	$\eta$

two parts, the aero-dynamical efficiency of the turbine  $\eta_{aero}$  and the bearing efficiency,  $\eta_{Bearing}$ ;

$$\eta_{mech} = \eta_{aero} \cdot \eta_{Bearing} \quad (3.4)$$

If the bearing losses are known, the aerodynamical efficiency of the turbine can be computed. The bearing losses can be estimated from known bearing characteristics or by measuring the bearing losses in a special rig, but the uncertainty in the measured data and thereby also in the estimation of the bearing losses, is high. This will make it difficult to compare the computed efficiency against measured data, since the computed efficiency is the aerodynamical efficiency while the efficiency based on measurements includes the bearing losses.

### 3.2. The stator

A radial turbine comprise of two essential parts, the stator and the rotor. The stator takes the flow from the exhaust manifold of the engine, accelerates and distributes it around the periphery of the rotor. The stator itself consists of a volute and in some cases a nozzle. The design of the volute is critical, since it determines the inlet flow conditions to the nozzle and the rotor. The volute can be of a single or a multiple entry type. For automotive turbochargers, the single entry turbine is so far the most common type. A single entry volute is shown in Figure 3.1. Twin entry turbines, with a meridional divider, see Figure 3.2, are used on commercial diesel engines, but also for smaller automotive engines. The advantage of this type of system is that exhaust manifold can be divided, resulting in a better scavenge process due to less interference between the various cylinders, which give less rest gases in the cylinders. A single

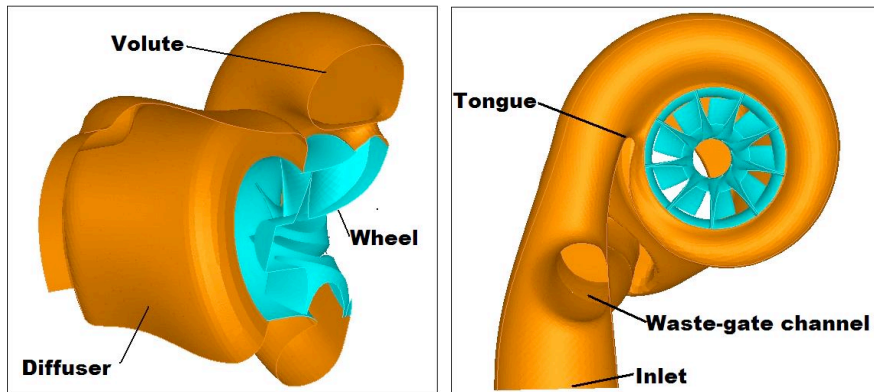


FIGURE 3.1. The different parts of a nozzle-less single scroll turbine.

entry turbine has higher swallowing capacity, and therefore lower pressure ratio for a given mass flow and the pumping losses of the engine will be lower. However, by using a twin-entry turbine a higher turbine pressure ratio can be reached in a shorter time and better utilization of the energy in the pulse, which improve the transient response of the engine. The drawback is that the twin-entry turbine has lower efficiency compared to single entry turbine, which has been showed by Capobianco & Gambarotta (1993). They measured the performance of a twin-entry turbine working under non-pulsatile and pulsatile flow conditions and compared the performance with an equivalent single entry turbine, and the efficiency was up to 5% lower for the twin-entry turbine for the non-pulsatile cases. Capobianco and Gambretta concluded that the lower efficiency was due to losses over the dividing tongue and losses in the shear layer between the flows leaving each entry. Yeo & Baines (1990) measured the shaft power for a twin entry turbine for different mass flow ratios in the two different entries, and computed the isentropic efficiency. The conclusion was that the lowest efficiency occurred when one of the two entries was fully closed, due to unfavourable incidence angle of the flow into the wheel. The incidence angle also varied in the axial direction at the inlet to wheel for this flow case, while the incidence angle was fairly constant in axial direction for equal mass flow in the two entries.

For turbines that are required to operate at high expansions ratios or high specific work output, a nozzle with vanes is required to turn the fluid, since a volute with nozzles will have better efficiency than a nozzle-less volute at these flow conditions. The nozzle, which is located between the volute and the wheel, consists of an annular ring of vanes which set the incidence angle of the working gas to the rotor and, in conjugate with the volute, further accelerate the fluid.

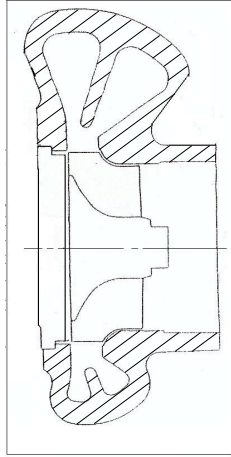


FIGURE 3.2. The volute for a twin-scroll turbine.

This implies that for a given flow capacity the volute with a nozzle can be smaller for a given acceleration and turning of the fluid. Nozzle-less volutes have the advantage to be simpler and cheaper, but the disadvantage that the relative inlet angle to wheel will not be uniform around the wheel, leading to deterioration of the efficiency due to increased incidence losses according to Winterbone *et al.* (1991). Spence *et al.* (2007) conducted an experimental investigation to compare the performance of vaned and vane-less volutes. They used three vane-less and three vaned volutes and for all the tested volutes, the same turbine wheel and diffuser was used. For each vane-less volute, which was designed for a specific pressure ratio, a corresponding volute with vanes was designed. They tested the different designs in non-pulsatile flow for pressure ratios over the turbine from 1.2 to 3.6, and the results show that the vane-less stators gave the best efficiency at all tested operation points. At the design points, the efficiency advantage was between 2% and 3.5%.

For spark ignition (SI) engines designed for passenger cars, the wide operating range of the IC engine implies that the turbocharger is matched for a relative low engine speed and to limit the pressure ratio over the turbine at high engine speeds, parts of the exhaust gases are by-passed the turbine wheel by opening the waste-gate valve. This also limits the shaft power developed by the turbine, and hence, limiting the pressure at the inlet to the IC engine. A more advanced way to extend the operating range of the turbine is

to use a variable turbine (VT). This can be done in two ways; one is to change the geometry of the volute (Variable Geometry Turbine, VGT) and the other approach is to use a variable nozzle (Variable Nozzle Turbine, VNT). Until recently, VNT have only been used for small and medium sized diesel engines, since a variable turbine can be used to get the correct pressure ratio between the air inlet system and the exhaust system to enable the use of an Exhaust Gas Recirculation (EGR) system. EGR is a key technology to reduce the  $NO_x$ -emissions of a diesel engine. For SI engines, the high exhaust temperature has limited variable turbines so far due to thermal expansion and durability, but at later years, variable turbines are also available for SI engines. There are different mechanical designs to change the geometry of the volute. One is to use a moveable sidewall of the volute to change the geometry of the volute, see for example Chapple *et al.* (1980). Since this mechanical solution has some problems there are very few or no radial turbines based on this design available for automotive applications on the market. Other ways of changing the geometry is to use a flap valve at the tongue of the turbine, which will control the swallowing capacity of the turbine. A flap valve can also be used to direct the flow to either an outer larger scroll or to an inner smaller scroll as shown in Figure 3.3.



FIGURE 3.3. A Variable Geometry Turbine concept, from Andersen *et al.* (2006).

Another way to extend the operation range is to change the geometry of the nozzle. A moveable wall can be used to change the area of the nozzle. Rogo *et al.* (1986) investigated several moveable wall variations for a turbine with nozzles and concluded that a moveable sidewall is a viable design. The drawback with this design is that the moveable wall introduces losses due to leakage at the movable wall. The nozzle area can also be changed by pivoting the vanes in the nozzle, see Figure 3.4. The VNT turbine investigated by Capobianco & Gambarotta (1992) was of this type, and the comparison of the non-pulsatile performance for a VNT and a VGT turbine showed that the peak



FIGURE 3.4. The variable vanes in nozzle for Variable Nozzle Turbine, from Andersen *et al.* (2006).

efficiency was lower for VT compared to a fixed turbine. This is most likely due to losses that the variable geometry systems induce due to leakage, wake losses behind the guiding vanes, separation, shocks and incidence losses, according to Capobianco & Gambarotta (1992) and Fukaya *et al.* (2000). But, the VT showed better efficiency over a wider range, and of the two tested variable turbines, the VNT had the best efficiency. Andersen *et al.* (2006) investigated the performance of five different VNT and one VGT with the approximately same swallowing capacity, and they concluded that the VGT turbine is the most suitable variable turbine type for spark ignition engines. Some of the VNT had better efficiency at lower mass flow rates, but the VGT turbine had the best performance at high mass flow rates. They also investigated the cold start emissions for all the tested variable turbines, and they concluded that a VT most likely requires better exhaust after-treatment system than a fixed single scroll turbine. The reason for the poor cold start emissions is the larger mass and heat-transfer area. Due to lower efficiency at low mass flow rates compared to a fixed geometry turbine, an IC engine with a VT will have larger pump losses at low engine rotational speeds, but this is compensated by the higher boost pressure that can be achieved by a VT at low engine rotational speeds. A VT will also give better transient performance of the engine. The turbocharger lag can also be decreased with VT which has been shown by Filipi *et al.* (2001).

Despite the many advantages with variable turbines, the most common type used on IC engines for passenger cars is the nozzle-less single-entry wastegated radial turbine due to the robust design and the relative low cost.

### 3.3. The rotor

The rotor design is a compromise between aerodynamic performance, durability, weight and inertia and manufacturing cost. A rotor with low weight and inertia will respond fast to changes in load, but in order to reduce the weight, the rotor must be small, which leads to high velocities and sharp curvatures, which in turn decreases the aerodynamic efficiency. A design for good efficiency requires large blade passage areas to limit the gas velocity and small curvature of the blades to avoid separation and secondary flows. The specific work output of the turbine can be expressed with the Euler turbo-machine equation:

$$W_{Shaft} = U_1 \cdot C_{\theta 1} - U_2 \cdot C_{\theta 2} \quad (3.5)$$

where  $C_\theta$  is the tangential velocity component of the gas at the inlet and outlet, respectively.  $U_j$  is the blade speed,  $U_j = r_j \cdot \omega$ . Station 1 is located at the rotor inlet and Station 2 at the rotor outlet, see Figure 3.5. For given rotational speed and radius, the maximum work output is achieved when the inflow tangential velocity component is high and the flow leaves the rotor in the axial direction.

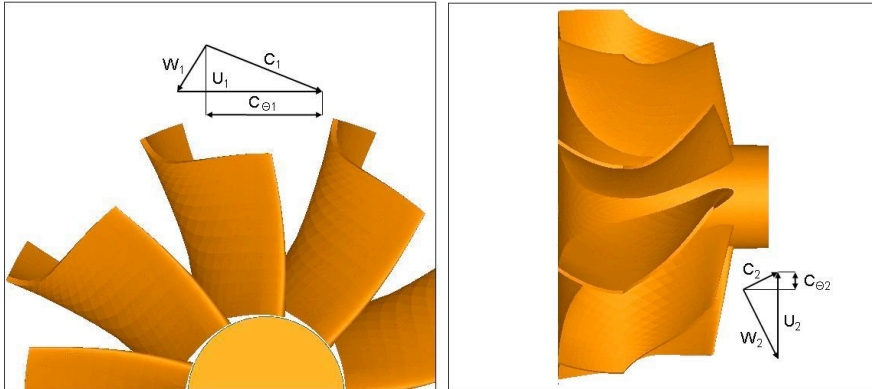


FIGURE 3.5. Rotor inlet (left) and outlet (right) velocity triangles.

A conclusion from the Euler turbo-machinery equation (3.5) is that the optimum velocity at the inlet to the rotor is a pure tangential velocity, but it has been showed that this is not the optimum inlet angle. Moustapha *et al.* (2003) concluded that the optimum relative inlet flow angle is in the region  $-40^\circ$  to  $-20^\circ$  while Spence & Artt (1998) showed that a 99 mm radial turbine was reasonably tolerant to relative incidence angles between  $-40^\circ$  to  $+30^\circ$ . An angle of incidence is positive when the inlet velocity tends to impinge on the blade tips at the pressure side of the blade. If the flow is more or less radial, it

will separate at the leading edge of the suction side, and a recirculation zone will be formed. If the inflow angle is more negative than approximately  $-40^\circ$  the flow will separate at the leading edge of the pressure side as shown in Figure 3.6.

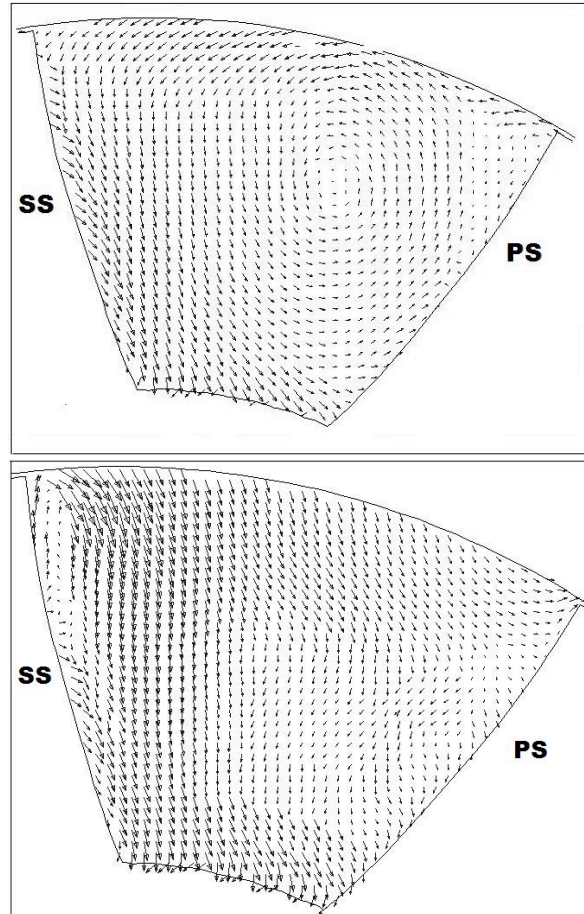


FIGURE 3.6. In-plane velocity components showing the tip vortex at the leading edge of the blade. Top figure: Relative inlet angle is approximately  $-65^\circ$ . Bottom figure: Relative inlet angle is approximately  $20^\circ$ .

The efficiency will also be higher if the exit flow of the wheel have no or slightly negative swirl according to Flaxington & Swain (1999). There are very few available articles in the open literature that discuss how to optimize the design of the wheel. This might depend on the low component cost for automotive

turbochargers, which imply the manufacturers use the cut-and-try techniques (Flaxington & Swain (1999)), and therefore they have large databases for different designs. Doran *et al.* (2001) studied the effects of different shroud profiles at different operating points. In their experimental study, they used four different shroud profile radius for a 99.0 mm radial inflow nozzle turbine. The results showed that the largest shroud radius gave the best performance under most conditions, but at the highest rotational speed, the most shaped shroud profile gave 3.5 percent points better efficiency. They also performed one dimensional numerical analysis to examine the effect of shroud profile with respect to incidence angle. For negative incidence angles, a small radius of shroud curvature gave the best performance, while for positive inlet angles, the largest radius gave the best performance. No measurements or 3-dimensional numerical computations were conducted in order to explain the effects of different shroud profiles.

Another way to increase the efficiency of the turbine is to use back swept blades, which has for example been showed by Barr *et al.* (2006) by a numerical study for a turbine with an inlet tip diameter of 90 mm. They studied three different back sweep blade angles;  $0^\circ$ ,  $15^\circ$  and  $30^\circ$ . At design condition, the efficiency was almost equally, while at off-design conditions, the efficiency was improved by 2% for the  $30^\circ$  back sweep angle blade due to a strongly reduced tip vortex at the leading edge. The drawback of this design is that it increases the bending stresses in the blade, and therefore limits the used of back swept blades. Palfreyman *et al.* (2002) studied the performance of four different turbine wheel geometries for a mixed flow turbine, and they concluded that a reduced chord length (with 18.75%) gave the largest deterioration of the efficiency, followed by a reduced number of blades (from 12 to 10), and then changing the inlet blade angle. The size of the gap between the blade tip and shroud also affects the efficiency, since the pressure gradient over the blade drives the flow over the tip and a jet and a tip vortex is created. Futral & Holeski (1970) performed an experimental study with the objective to study the effects of tip clearance for a radial turbine. The wheel diameter was 152.9 mm, which is quite large compared to the size of the wheel of an automotive turbocharger. Tip clearance values of 0.25 to 7% of the passage height at the rotor entrance and at the rotor exit were used. The results showed that an increase of the axial tip clearance at the rotor entrance gave a decrease of the total efficiency of 0.15% for each percent increase of tip clearance. At the exit of the rotor, an increase of the radial tip clearance from 1% to 3% of the passage height gave a decrease of the efficiency of 1.6% for each percent increase of tip clearance. For the range of 3% to 7% the decrease of efficiency was smaller, but still, larger than the effect of increasing the radial gap at the entrance. But, the tip clearance height is not the only parameter that affects the flow over the

tip, and hence, the tip vortices and the losses that they introduce. Dambach & Hodson (2001) conducted an experimental investigation of the flow over the blade tip for different axial and radial tip-clearances for a radial turbine. The tip gap was varied from 0.6% to 1.2% of the local blade height. They showed that different blade tip gap height to blade width ratio gave different behaviour for the tip leakage flow. If the ratio was below approximately  $\frac{1}{6}$ , the tip leakage flow was mixed with the boundary layer at the shroud, resulting in a tip leakage flow with low momentum, and hence, a less strong tip vortex at the suction side. If the ratio was larger than approximately  $\frac{1}{6}$ , the inertia effects dominated over the viscous effects, and the momentum of tip leakage flow from the pressure to suction side was higher, resulting in a stronger tip vortex. Also, they showed that the pressure difference over the gap remains relatively constant for the tested tip gap heights.

For turbines working in pulsatile flow, mixed flow turbines have some advantages compared to radial turbines. A mixed flow turbine is a turbine, with its leading edge of the blade inclined to the axial axis. This implies that the flow at the entrance to the wheel have both an axial velocity component and a radial velocity component. At higher mass flow rates, which is the same as higher pressure ratio and lower  $U/C_s$ , mixed flow turbines have better efficiency compared to radial turbines due to less turning of the flow in the wheel. The turning process from the radial inlet to the axial outlet gives raise to losses due to secondary flow. The  $U/C_s$  ratio is called the blade speed ratio, and  $U$  is the rotor tip speed and  $C_s$  defined as:

$$C_s = \sqrt{2 \cdot c_p \cdot T_{01} \cdot \left(1 - \frac{p_2}{p_{01}}\right)^{\frac{\gamma-1}{\gamma}}} \quad (3.6)$$

Mixed flow turbines have the maximum efficiency at a  $U/C_s$  ratio of approximately 0.65, while a radial turbines have the best efficiency at blade speed ratio of approximately 0.7 (Chen *et al.* (1997)). The efficiency also drops substantially for  $U/C_s$  values below 0.7 for radial turbines, while mixed flow turbines can maintain high efficiency over a larger region of lower  $U/C_s$  ratios.

### 3.4. Turbine performance under pulsatile flow

As already mentioned, the flow in the exhaust system of an IC engine is highly pulsatile, and this affects the performance of the turbine. The performance of turbines working under pulsatile flow conditions has been assessed by many researches by both different numerical methods and by experiments. A typical feature of turbines working in pulsatile flow is that when plotting the mass flow versus shaft torque, as been done in Figure 3.7, the trajectory form a closed loop, enclosing the quasi-stationary trajectory. The same is valid when plotting the blade speed ratio  $U/C_s$  versus the efficiency.  $U/C_s$  varies during the pulse,

since the rotational speed of the rotor is almost constant, whereas the variation of  $U/C_s$  is from low values of approximately 0.2 to high values above 1 (when the pressure ratio is equal to one, the isentropic velocity will be zero), which is far away from the optimal value of approximately 0.7.

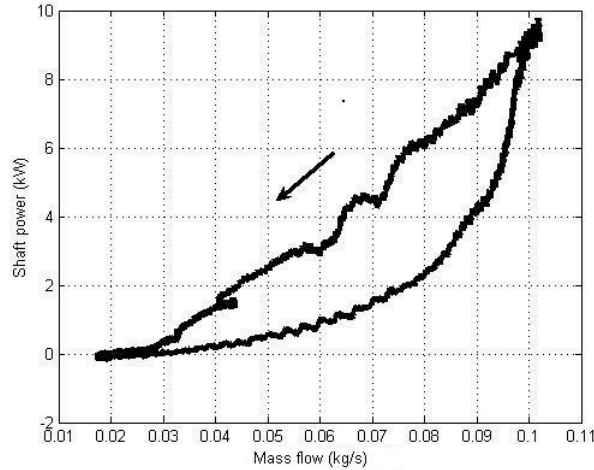


FIGURE 3.7. Computed shaft power vs. mass flow at inlet.

For turbines operating under pulsatile flow conditions, the mean efficiency is lower compared to non-pulsatile flow conditions for the same mass flow and pressure ratio, but the instantaneous performance can be both higher and lower, see for example Winterbone *et al.* (1990), Winterbone *et al.* (1991), Dale & Watson (1986) and Capobianco & Gambarotta (1990). But it must be emphasized that it is very hard to compute the isentropic efficiency in an accurate way, due to the phase shift between pressure and mass flow and the time it takes for the energy to propagate from the measuring point to the turbine wheel. It is also hard to measure the time dependent shaft power.

Winterbone *et al.* (1991) investigated the performance of a radial turbine in both non-pulsatile and pulsatile flow. The frequency of the pulsatile flow was 35 Hz. To measure the time dependent shaft power, they used an hydraulic dynamometer in combination with the knowledge of the varying angular velocity. The time resolved shaft torque is then the sum of the mean shaft torque obtained from the hydraulic dynamometer and the product of the moment of inertia of the rotating part and the time derivate of the angular velocity. By analyzing the measured pressure distribution around the volute for both non-pulsatile and pulsatile operating conditions, they concluded that the flow in

the turbine volute can be treated as being quasi-stationary, since the rate of change of pressure with respect to distance was much greater than it was with respect to time. Since the shaft torque measurements were time-resolved, they could compare them to the time resolved pressure traces at the inlet, and the phase lag between the pressure trace and the torque trace was about  $40^\circ$ . The time this phase lag corresponds to, is larger than the pressure wave travel time from the inlet to the rotor, and hence the phase lag do not only depend on the wave propagation time. Winterbone *et al.* also reported that the mass flow pulses were approximately in phase with the pressure pulses, but the mass flow trace was quite noisy, so it was hard to determine any phase shift. The rotational speed of the wheel varied with approximately 2% during the pulse. Wallace *et al.* (1969) investigated the effects of different frequencies, mass flows and turbine speeds. They used a dynamometer to measure the shaft torque of the turbine, and this dynamometer could be operated up to 100 000 rpm. The frequency of the pulsatile flow was varied from 16.7 Hz to 50 Hz, and they concluded that the turbine shaft torque first increased and then decreased with increasing frequency. The shaft power diminished slightly with increasing mass flow for constant rotational speed of the turbine wheel and mean inlet pressure to the turbine. Benson & Scrimshaw (1965) conducted experiments where the pulse frequency was varied from 30 Hz to 70 Hz, and the rotational speed of the turbine wheel was varied from 30 000 rpm to 60 000 rpm. The used turbine was a nozzled radial turbine with twin entries. The results showed also that the efficiency increased up to a pulse frequency of 60 Hz, and then decreased with further increase in pulse frequency.

Dale & Watson (1986) measured the shaft power of a twin entry turbine working in pulsatile flow. They concluded that the efficiency varied with varying admissions in the two entries, where the lowest efficiency occurred when the flow entered only one of the two entries. For an operation point with a pulse frequency of 40 Hz, the maximum deviation of the instantaneous efficiency from the quasi-stationary assumption was up to 10%, with both higher and lower values than the efficiency from the quasi-stationary assumption. Karmanis *et al.* (2001) concluded from an experimental study, that the deviation of isentropic efficiency from the quasi-stationary assumption was reduced as the pulse frequency was increased for a mixed flow turbine. The frequency of the pulsatile flow was 40 Hz and 60 Hz, respectively. When they computed the isentropic efficiency, they applied a correction for the phase lag, which corresponded to the sonic travel time from the inlet to the wheel. The cycle-averaged efficiency was lower than the corresponding steady-state efficiency, due to the large variation of flow conditions. The incidence angle varied from  $-80^\circ$  to  $40^\circ$  during the pulse. In the experiment conducted by Arcoumanis *et al.* (1999) the steady and unsteady performance of a mixed flow turbine was investigated

for different rotational speeds of the wheel and with pulse frequencies of 40 Hz and 60 Hz. The results showed that the cycle averaged isentropic efficiencies were higher for a mixed flow turbine compared to a radial turbine. By using a cycle averaged efficiency, no phase shifting of the shaft torque is needed, which is beneficial, since the time-resolved isentropic efficiency is strongly affected by the size of the phase shift.

Lam *et al.* (2002) performed a time resolved 3-dimensional numerical study of the pulsatile flow in a radial nozzleed turbine. They used the frozen rotor technique to model the rotation of the wheel. The results showed that instantaneous performance of the rotor under pulsatile conditions did not vary significantly from the non-pulsatile conditions, and Lam *et al.* concluded that the wheel can be treated as a quasi-steady device, while the volute must be treated as a non quasi-stationary flow device. Palfreyman & Martinez-Botas (2005) investigated the pulsatile flow in a mixed flow turbocharger with numerical methods. They used a medium sized mixed flow nozzle-less turbine. They concluded that the used method with explicit rotation of the wheel, better captures the non quasi-stationary behaviour of the turbine than the method used by Lam *et al.* (2002). But, this might also be an affect of that Palfreyman and Martinez-Botas used a nozzle-less turbine, without the damping the nozzles can introduce, leading to a more uniform flow into the rotor. At the inlet to the rotor, the incidence angle varied from  $-92^\circ$  to  $+60^\circ$ , which will give raise to losses, due to strong tip vortices at the leading edge of the blades. The blade torque and the work output fluctuated substantially and with the frequency of the pulse. A perturbation with same frequency as the blade passage frequency was also superimposed on the shaft torque trace, which is an effect of the blades passing the tongue. The velocity field within the turbine wheel also varied substantially during the pulse due to poor flow guidance at the entrance to the turbine wheel. The trajectory of the mass flow versus efficiency showed a hysteresis loop, which encapsulates the quasi-steady values. This is, according to Palfreyman and Martinez-Botas, due to the imbalance between inlet and outlet mass flow during the pulse and the “filling and emptying” of the volute as the turbine acts as a restriction. They also reported a phase lag between the computed isentropic work and the actual work.

One way to increase the work output of a turbine working in pulsatile flow is to use some type of active control of the turbine. This can be done by controlling the throat inlet area to the wheel in accordance to the exhaust pulse. This improves the pressure ratio, especially at low mass flow. Pesiridis & Martinez-Botas (2006) tested a mixed flow turbine with a nozzle that was able to alter to the throat inlet area to the turbine wheel. The variable nozzle was of a sliding-wall type restrictor and it was possible to control the throat area in phase and out of phase with the incoming pulses. The actuator was

an electrodynamic shaker. Tests were performed at two different frequencies of the pulsatile flow. Different phase settings between the pressure pulse and the movement of the nozzle were also tested. An increase in shaft power output with up to 7% was achieved with the active control system, but the efficiency was lower for the turbine fitted with this type of active control system. A better design is to active control the incidence angle of the vanes in a vaned nozzle. Rajoo & Martinez-Botas (2007) studied the performance of mixed flow turbines with moveable nozzle vanes. The movement of the nozzle vanes was controlled in both a passive way and in an active way with an actuator. In the passive system, an increasing pressure in the volute opened the vanes against a pre-loaded spring, and when the pressure decreased, the vanes were retracted. In this way, an increased area is obtained at high pressure, while the area is decreased at lower pressure. The passive system increased the shaft power output (with 36% for the best case) during the period of the pulse when the mass flow was low, but reduced the maximum power. The cycle averaged power was lower compared to a turbine with fixed vanes. Still the efficiency was better for the turbine with a passive control system. For the active system, with a forced movement of the vanes, a small improvement of the efficiency was achieved. The authors also concluded that of the tested control systems, a passive system with moveable nozzle vanes is probably the most beneficial system, especially for IC engines working with a narrow speed range.

When computing the isentropic efficiency and  $U/C_s$ , it is common to assume that the pressure at the outlet of the turbine is constant during the pulse. This assumption can be doubted; special for small turbines with a size that is common for automotive applications. Capobianco & Marelli (2005) investigated the unsteady pulsatile flow in a four to one exhaust manifold and a nozzle-less radial turbine, and one of the conclusions was that the flow unsteadiness at the turbine outlet cannot be neglected due to the fact that the measured pressure downstream of the turbine was not constant over a pulse period. The amplitude of the pressure variations was approximately 0.3 bar, and the amplitude of the pulse at the inlet to the turbine was for this case approximately 1.0 bar. The amplitude of the pressure variations downstream of the turbine also increased when the waste-gate valve was opened, since the maximum pressure before the turbine was higher, due to an increased mass flow through the system. Capobianco & Gambarotta (1990) also studied the effects of different waste-gate valve opening areas on the pressure pulses upstream and downstream of the turbine, and the results showed that the pressure pulses at the turbine inlet were unaffected by the waste-gate valve opening, while the pressure at the outlet of the turbine had a high frequency oscillation superimposed. The frequency was about 3 kHz, but since neither the blade number nor the rotational speed of the wheel was specified in the report, no conclusion of

the source can be made. Benson (1974) also noticed pressure fluctuations downstream of the turbine diffuser for pulsatile inlet conditions. He also concluded that the non-steady performance of the turbine deviates from the quasi-steady assumption. He based his result on measurements of the turbine performance from both non-pulsatile and pulsatile inlet conditions.

The only time resolved three-dimensional numerical investigation of the flow field and the performance of radial turbines working at rotational speeds that are common for small automotive IC engines that has been found in the available literature has been performed by Lam *et al.* (2002). In their study, they used time resolved three-dimensional numerical computations to investigate the performance of a nozzled radial turbine with a rotor tip diameter of 47.04 mm. They only investigated one operational point, where the frequency of the pulsatile inlet flow corresponded to engine speed of 1600 rpm and the turbine rotational speed was set to 136 000 rpm. The tip gaps between the blades and the shroud was neglected, which of course affects the accuracy of the results. They also used the “frozen rotor” wheel modelling approach, which imply that blade passage effects are not taken into account. No investigations of the influence of different frequencies and amplitudes on the time-resolved three-dimensional flow field and the performance of radial turbines working at rotational speed in the range of approximately 80 000-300 000 rpm has been found. Therefore, a numerical study has been performed to investigate the effects of different frequencies and amplitudes of the pulsatile flow at the turbine inlet. The results from the time-resolved three-dimensional computations have been analyzed with focus on the turbine performance and the flow field. For these computations, the secondary flow at the inlet was neglected. To assess the effects of secondary flow at the inlet, a numerical study has also been performed with different perturbations applied at the inlet to the turbine. The different cases and the results are presented in Chapter 5.

## CHAPTER 4

### Methods

This chapter will start with a very brief overview of the governing equations; the continuity equation, the momentum equation and the energy equation. These equations form a model of incompressible and compressible flows of gases and liquids. These equations are non-linear, and there exist only a few laminar flow cases where these equations can be solved analytically. Instead, one can use numerical techniques to solve the governing equations, which will also be briefly discussed in this chapter.

#### 4.1. Governing equations

The governing equations that describe the conservation of mass (4.1), momentum (4.2) and energy (4.3) are the Navier-Stokes (NS) equations and the energy equation complemented with the equation of state (4.4):

$$\frac{\partial \rho}{\partial t} + \frac{\partial}{\partial x_j}(\rho \cdot u_j) = 0 \quad (4.1)$$

$$\frac{\partial}{\partial t}(\rho \cdot u_i) + \frac{\partial}{\partial x_j}(\rho \cdot u_i \cdot u_j) = -\frac{\partial p}{\partial x_i} + \frac{\partial \tau_{ij}}{\partial x_j} + \rho f_i \quad (4.2)$$

$$\frac{\partial}{\partial t}(\rho \cdot h) + \frac{\partial}{\partial x_j}(\rho \cdot u_j \cdot h) = \frac{\partial p}{\partial t} + u_j \frac{\partial p}{\partial x_j} + \tau_{ij} \frac{\partial u_i}{\partial x_j} - \frac{\partial q_j}{\partial x_j} + W_{ext} + q_H \quad (4.3)$$

$$p = \rho \cdot T \cdot R \quad (4.4)$$

where  $\rho$  is the density,  $p$  the pressure,  $T$  the temperature,  $x_i$  the cartesian coordinates,  $t$  the time,  $\mathbf{U} = u_i$ ,  $i=1,3$  is the velocity,  $f_i$  the specific force,  $\tau_{ij}$  is the viscous shear stress tensor,  $h$  is the specific enthalpy,  $R$  is the gas constant and  $q_i$  is the heat flux.  $W_{ext}$  is the work of external volume forces and  $q_H$  is the heat source. The heat flux  $q_i$  is modelled through Fourier's law. The viscous shear stress tensor,  $\tau_{ij}$  is defined as:

$$\tau_{ij} = \mu \cdot \left( \frac{\partial u_i}{\partial x_j} + \frac{\partial u_j}{\partial x_i} - \frac{2}{3} \delta_{ij} \cdot \frac{\partial u_k}{\partial x_k} \right) \quad (4.5)$$

## 4.2. Turbulence

When the flow reach a certain Reynolds number the flow goes from being laminar to turbulent. The Reynolds number is defined as

$$Re = \frac{U \cdot L}{\nu} \quad (4.6)$$

where  $U$  is a characteristic velocity scale,  $L$  is a characteristic length scale and  $\nu$  is the kinematic viscosity. Reynolds number is a dimensionless number that describes the ratio between the inertial forces and the viscous forces. This means that for low Re-number, the viscous forces are the predominant, and for high Re-number, the inertial forces are dominant. For a pipe flow, the characteristic velocity is the bulk velocity and a typical length scale is the pipe diameter. With these characteristic quantities, a laminar pipe flow will become turbulent when the Re-number exceeds a certain value which depends on the particular set-up; i.e. approximately 2000 or larger, c.f. Carpinlioglu & Gundogdu (2001). One may define a *critical* Re-number based either on theoretical (stability analysis) arguments or empirical data as is the case for the pipe flow. Flows with Re-number larger than the critical Re-number, does not necessarily imply that it is a fully developed turbulent flow. Turbulent flows are characterized by being time dependent and 3-dimensional where the flow at each location can be described by a mean velocity and a fluctuating part. Since the fluctuating part is irregular, only statistical methods can be used to characterize and quantify the flow properties. Another feature of turbulent flow is that the viscous forces dissipate the turbulent kinetic energy into heat. The turbulent flow consists of eddies with different length scales, where the largest eddies are the most energetic ones. The large eddies have velocity and length scales of the same order as the mean flow. The large eddies are unstable and break up into smaller eddies. These smaller eddies in turn drive even smaller eddies, until the scales where viscous dissipation becomes important. In this way, energy is transferred from the larger scales to the smaller scales. Small eddies are by nature independent of the boundary conditions and therefore have a universal and isotropic character. The larger eddies are characterised by the particular flow and these eddies carry most of the turbulent kinetic energy. In the range between the energy bearing eddies and the small eddies, in the dissipative range, one finds a range of eddies (scales) that are dependent only of inertia and therefore one talks about the inertial subrange. The dominating part of turbulence production takes place in the energy containing range, while almost all dissipation occurs in the dissipation range. The transfer of energy from larger to smaller scales occurs mainly in the inertial subrange.

### 4.3. Numerical methods

Since the NS equations are non-linear, no general analytic solution exists; instead, numerical techniques can be used. By using a discretization practice, the NS equations are transferred into a system of non-linear algebraic equations which than can be solved numerically. There are three main discretization methods that are used for fluid problems; the finite difference (FD) method, the finite element (FE) method and the finite volume method (FV). In all numerical studies presented in this thesis, the commercial general CFD solver STAR-CD ver. 3.26 has been used. This code is based on the FV methods.

For the temporal discretization, two different schemes have been used, a first order implicit scheme and the Crank-Nicholson scheme. The implicit scheme has in principle no restrictions on the time step  $\delta t$ , but it must be small enough so as to resolve the fluctuations and additionally to limit the temporal approximation errors. The Crank-Nicholson scheme is of formal second order accuracy, but as for all central second-orders schemes, it is liable to introduce non-physical oscillations when the viscous smallest scales are not fully resolved. The Crank-Nicholson scheme can be blended with an implicit scheme. This will then lead to a reduction in the formal order of accuracy of the numerical scheme but with the gain of enhanced stability. When determining the size of the time step it is important to consider the coupling to the spatial discretization and the speed which the information is propagating with (i.e. the local physical properties of the flow). This means that time step must be small enough to ensure that information can not propagate no more than over a computational cell  $\delta x$  during a time step  $\delta t$ . This condition allows the numerical scheme to track the propagation of physical information and it is expressed in numerical analysis in form of the Courant condition (*CFL*) number that must be below 1:

$$CFL = \frac{|U| \delta t}{\delta x} \leq 1 \quad (4.7)$$

where  $U = u \pm c$  is the physical propagation speed, with  $c$  being the speed of sound and  $u$  the convection velocity.

For the approximation of the spatial discretization of the convection terms, different schemes are available in the used code. Three of them have been used, the first order Upwind Differencing (UD) scheme, the formal second order Monotone Advection and Reconstruction Scheme (MARS) and a blended Central Differencing (CD) scheme. The UD scheme is known to preserve the physical bounds of the fluxes, but can in many cases lead to numerical diffusion. A second order scheme will better preserve steep gradients, but can also introduce non-physical oscillations, known as numerical dispersion. The MARS scheme employs a Total Variation Diminishing (TVD) scheme, making

it particularly well suited to capture the strong gradients expected for these cases. Since the MARS scheme is proprietary to CD-adapco, no details of the scheme can be found in the open literature. According to CD-adapco (2005) this scheme is the scheme that is least sensitive to solution accuracy to mesh structure and skewness of the available schemes in the used code. Since the details of the scheme are not known we have made extensive tests to assess its accuracy for problems of relevance to engine flows.

A modified version of the Pressure-Implicit with Splitting of Operators (PISO) method proposed in Issa (1986), Issa *et al.* (1986) and Issa *et al.* (1991) is implemented in the used code to solve the discretized governing equations at each time step. One of the major differences is that the number of corrector stages is not limited to two, as being proposed in the original version; instead, the number of corrector stages is determined by the splitting error, which will, according to CD-adapco (2005), increase the accuracy and reliability of the method.

#### 4.3.1. Turbulence modelling

To resolve all scales of the turbulent flow the grid size and the time step must be smaller than the smallest length and time scale of the flow. This can be done by fully resolved simulations, Direct Numerical Simulation, and in general, the computation cost will be proportional to  $Re^3$ . This approach is not feasible for the applications studied in this work, since the required computational resources are not available yet. Instead, the governing equations can be handled by two other methods, the Reynolds Averaged Navier Stokes (RANS) approach and the Large Eddy Simulation (LES) approach. In the RANS approach, the governing equations are expressed in terms of the mean quantities. The base line of the RANS equations is that the instantaneous flow field can be divided into a time averaged part and a fluctuating part. With this inserted in the governing equations and averaged over time, the RANS equations are obtained, which describes the time averaged flow field. Due to the non-linearity of the NS equations, additional terms appear in the RANS equations; the Reynolds stresses,  $\overline{u'_i u'_j}$ . These terms represent the effect of the fluctuations on the mean field. The Reynolds stresses cannot be expressed analytically in terms of the mean variables and hence they have to be modelled in order to close the equations. Turbulence models can be divided in several major categories, such as Eddy viscosity models and Reynolds stress based models. The eddy viscosity models are based on the turbulent-viscosity hypothesis which relates the Reynolds stresses to the mean velocity field as:

$$\overline{u'_i u'_j} = \frac{2}{3} k \delta_{ij} - \nu_T \left( \frac{\partial U_i}{\partial x_j} + \frac{\partial U_j}{\partial x_i} \right) \quad (4.8)$$

where  $k$  is the turbulent kinetic energy and  $U_i$  is the mean flow velocity components. To close this equation the turbulent viscosity,  $\nu_T$  has to be expressed in terms of the mean quantities. The most common turbulence models are the two equations models, which are based on transport equations. One of these models is the  $k$ - $\epsilon$  model, and in this model, the transport equations are solved for the turbulent kinetic energy and its dissipation  $\epsilon$ . From these two quantities, the turbulent viscosity can be determined by the relation:

$$\nu_T = C_\mu \frac{k^2}{\epsilon} \quad (4.9)$$

$C_\mu$  is a model constant. There are also other alternatives of the standard  $k$ - $\epsilon$  model, for example the Renormalisation Group (*RNG*)  $k$ - $\epsilon$  models, which has an additional term in the  $\epsilon$ -equation to take into account the effects of the mean flow on distortion of the turbulence. This model has been used for all the RANS computations presented in this thesis. In the Reynolds-stress models, model transport equations are solved for the Reynolds stresses,  $u_i u_j$  and for the dissipation,  $\epsilon$ . Since the Reynolds stresses are known, the turbulent-viscosity hypothesis is not needed. This has the advantage that effects of anisotropy of the turbulence, streamline curvature, swirling motions and high rate of strains are taken into account. Still, some terms in the Reynolds stress transport equations have to be modelled, with some more or less realistic assumptions. Unfortunately, there are no generally valid turbulence models. For plane boundary layer flow, most turbulence models work more or less well, simply since such simple flows are used for model calibration. On the other hand, the flow near a solid wall depends strongly on the shape of the boundary and the flow outside of the boundary layer. These effects make it difficult to have generally valid models. Treatment of the near wall turbulence is often done by using certain wall models. These models may work when the local flow conditions resemble those for which the model is calibrated for. The most common wall model, is the so called (standard) wall function, which is based on the log-law behaviour of the turbulent boundary layer on a plane wall at zero pressure gradient. Modifications to the logarithmic law of the wall to take into account effects of wall curvature and adverse pressure gradients have also been proposed. A more advanced wall model, is the so called two-layer model, where simplified turbulence models are used in the viscous region close to walls whereas high Re turbulence model is used further away from the wall.

In LES, the large scales of the turbulent flow are resolved while the smaller scales are modelled. This implies that the resolved flow field is, in general, 3-dimensional and time dependent. These properties of LES makes it a natural candidate for handling the pulsatile flow in the turbine. In LES, the dependent variables are low-pass filtered with a spatial filter. The filter width is defined through the smallest spatial resolution which can be related to the volume of

the computational cell,  $V_{cell}^{1/3}$ , i.e.  $\Delta = V_{cell}^{1/3}$ . The governing equations for the filtered variables have additional terms as compared to the original equations. These terms have to be expressed in terms of the filtered variables in order to close the equations. In the momentum equation, the term that has to be modelled is called the Sub-Grid-Scale stress (SGS-model). As for the RANS approach, different SGS-models exist, and the first proposed is the Smagorinsky model. In the Smagorinsky model, as in the RANS framework one introduces a modified viscosity and assumes that the effects of unresolved turbulence can be accounted for in analogy with the molecular viscosity. Thus, the total viscosity is the sum of molecular and SGS-viscosities:  $\nu = \nu_{Physical} + \nu_{SGS}$ .  $\nu_{SGS}$  is assumed to be proportional to the absolute value of the rate of strain tensor  $\bar{S}_{ij}$  and the filter width:

$$\nu_{SGS} = (C_s \cdot \Delta)^2 |\bar{S}_{ij}| \quad (4.10)$$

where  $C_s$  is a model constant. It has long been known that the Smagorinsky model is dissipative, especially in the near wall regions and when rotational effects are present. In analogy with the RANS-approach, one has also proposed a one equation eddy viscosity model, where a transport equation for the unresolved turbulent kinetic energy is solved. In this model,  $\nu_{SGS}$  is assumed to be proportional to the filter width and the unresolved turbulent kinetic energy:

$$\nu_{SGS} = C_k \cdot \Delta \cdot \sqrt{k_{SGS}} \quad (4.11)$$

One may argue against this model in addition to the simple fact that it has similar limitations as the Smagorinsky model. The small scales of turbulence are of local and universal character (i.e. independent on the particular problem due to their small scale, except close to the wall). Therefore the SGS effects should be expressed by local variables and not through an elliptic partial differential equation. Additionally, one may argue that the eddies of different scales interact with each other similarly if the scale ratio is similar. This is the foundation of several SGS models such as the scale similarity and dynamic models. In the SGS models based on the scale similarity hypothesis, the subgrid tensor is approximated by an analogous tensor computed from the smallest resolved scales, c.f. Bardina *et al.* (1980). In the dynamic models, the SGS model coefficients are based on the local properties of the flow field, which implies that the coefficients are functions of space and time, c.f. Germano *et al.* (1991) and Ghosal *et al.* (1995). Based on the same argument one may also claim the error in neglecting the SGS terms is of second order in the filter size. Thus, if the spatial resolution of the flow is high enough the SGS terms are small. In fact as the resolution is improved LES becomes DNS. With this in mind one may claim that for adequate resolution one may refrain

from using an explicit expression for the SGS terms. This is the foundation for the so called Implicit LES, sometimes called ILES or MILES=Monotone Implicit LES. The size of the SGS term is only one factor in the considerations related to the modelling of the SGS terms. The SGS terms represent the effect of the small scales on the large ones. They should account for a net energy transfer from the resolved scales to the unresolved dissipative ones. Instantaneously, they also act to transfer energy in the other direction, an effect that is known as backscatter and which has not been quantified. Since the smallest scales are unresolved the SGS model should account for the dissipation. When no explicit SGS model is used, one may utilize the inherent dissipative properties of the numerical scheme, provided that the dissipation of the larger scales is negligible. It should be, however, emphasized that the accuracy of these methods depends of the grid size and numerical schemes. A first order scheme implies that the cut-off frequency will be lower compared to a higher order scheme since the artificial viscosity (dissipation) is higher for first order schemes compared to second order schemes. But, for second order schemes, such as the central difference scheme, the odd derivative of the truncation error can introduce dispersion, which can result in non-physical oscillations in the flow field. The effect of these factors on the resolved scales is often small provided that the grid resolution is fine as compared to the resolved scales that are of interest. Marginally resolved flows may of course suffer from lack of accuracy since the numerical dissipation is proportional to the grid spacing. A measure of the local resolution can be assessed by considering the local turbulent energy spectrum and the extent of the resolved inertial subrange.

A disadvantage with LES is that the boundary layers have to be resolved to capture the dynamics in the near-wall regions. To be able to do this, the near-wall region must be resolved which results in a very large number of grid points. As in the RANS case, different wall models have been proposed and these can be divided into two categories:

- Modifying the SGS eddy viscosity in the region closest to the wall, for example a damping function of the viscosity or compute the eddy viscosity based on the logarithmic law of wall.
- Solve the one-dimensional boundary layer NS equations on a fine grid in the near-wall region. The fine grid can also be a “grid-within-the grid”, where a one-dimensional grid is included in the cell layer closest to the wall.

In this thesis, the Implicit LES approach is used for almost all cases, and hence, no near-wall model is used at all. For the case where the Smagorinsky model is used, a damping function is applied at the cell layer adjacent to the wall, where the filter width in this cell layer is defined as:

$$\Delta = \min(\kappa y, \sqrt[3]{Cell\ volume}) \quad (4.12)$$

$y$  is defined as the distance from the wall to the adjacent cell centre and  $\kappa$  is a constant.

#### 4.3.2. Wheel modelling

In the turbine, the turbine wheel is rotating in relative to the stationary turbine house. This can be modelled by two different approaches:

- The Rotating Reference Frame technique (RRF)
- Moving mesh technique.

In the RRF concept one uses a coordinate system that rotates with the turbine. Therefore, the Coriolis term is added to the Navier-Stokes equation. Since the housing of the turbine is not rotating, the computational domain contains also regions which are described in non-rotating coordinates. Hence the Coriolis terms are activated only in the region where rotation of the geometry occurs.

In the moving mesh technique, also called the Sliding Mesh (SM) technique, one part of the mesh is moving or rotating in relative to the stationary part. At the interface between the moving and the stationary part, the moving mesh is made to slide past the stationary part. At the sliding interface, the connectivity for cells on either side of the interface change at each time step. This is implemented in a way that there are no restrictions on the relative position of the cell faces on either side of the sliding interface, i.e. cell faces across the sliding interface do not to have a one-to-one correspondence. In order to preserve flux of mass, momentum and energy across the sliding interface and to avoid introducing non-physical perturbations, the interpolation over the sliding interface must be done in an appropriate way. The rotational speed of the wheel and cell sizes at the sliding interface will also determine the time step; the time step must be small enough to ensure that cells on both sides of the sliding interface do not pass each other completely during one time step.

#### 4.4. Numerical accuracy and uncertainty

All numerical techniques are based on discrete approximations of the dependent variables and thereby a discrete approximation to the governing equations. The discretization steps in both the time and space introduce errors. The errors can be divided in four groups:

- Errors due to modelling errors in the governing equations.
- Discretization errors, due to time and space discretization and the used discretised representation of the dependent variables.

- Errors in computing the discrete solution (i.e. convergence errors in the solution process).
- Errors due to round-off error due to a limited number of significant digits in the computations.

The influence of these different errors can be examined by performing numerical accuracy studies (using successively refined grids) and comparing the results from the computations against measured or computed data. In the latter case, data from DNS is often used.

The purpose of numerical accuracy studies is to state the order of accuracy of the used schemes. The numerical accuracy studies can also be used to compute the uncertainty of the results. To investigate the numerical accuracy and the uncertainty, the GCI-method proposed by Celik (2005) was used. The results from these studies show that the order of accuracy for the used code is between 1 and 2, depending on the flow case and the used turbulence modelling approach, see Paper 1 and Paper 2. This reflect the order of accuracy of the used schemes, where the formal second order MARS scheme is used for spatial discretization of the convection terms and a blended central difference scheme for the viscous terms. A blended Crank-Nicholson scheme was used for temporal discretization of the LES computations for the pipe cases and the first order Euler implicit temporal discretization and was used for the turbine computations and for the RANS computations. The GCI-method can also be used to estimate the uncertainty of the results. For the pipe-flow cases, the uncertainty of the computed velocity field at the finest grid was below 4% for the LES computations for the single bend case, and for the RANS computations on the double bend case the uncertainty was below 9.6% for the finest grid.

For pulsatile flow, the evaluated quantity must be phase averaged. The total number of samples can be computed with a formula given in Johansson & Alfredsson (1988) for a given a given sampling error  $\epsilon$ :

$$\epsilon(X) = \frac{1}{\sqrt{N}} \frac{x_{rms}}{X_m} \quad (4.13)$$

where  $N$  is the total number statistically independent samples,  $X_m$  is the mean value and  $x_{rms}$  is the root mean square value. Since the inflow conditions for the double bend pipe was pulsating, the velocities must be phase averaged in the LES computations, which implies that 400 cycles had to be computed if the sampling error should be below 1%, and hence no uncertainty has been computed for the pulsatile flow cases.

For the turbine computations, the numerical accuracy study was performed on simplified turbine geometry, where the complete wheel and only parts of the volute and the diffuser were modelled to reduce the computational time. The

rotational speed for the rotor was 97 897 rpm and a fixed mass flow was specified at the inlet.

TABLE 1. Computational accuracy study.

Grid number	Number of cells in the rotor	Averaged cell size (mm)	Shaft torque (Nm)	Pressure drop (kPa)
1	76 662	0.65	0.362	30.90
2	297 648	0.42	0.276	30.28
3	541 008	0.34	0.287	29.86
4	968 229	0.28	0.290	29.83

As can be seen in Table 1, the convergence for grid numbers 2, 3, and 4 is monotone and the uncertainty for the shaft torque for the finest grid is about seven percent and for the pressure drop 0.3%. The resolution for the computations for the complete turbine cannot be as fine as it was for grid 4 in the accuracy study, due to the computation time. The used grid for the complete turbine has the same resolution of the wheel region as grid number 2 in the accuracy study.

#### 4.5. Comparison of computed and measured data

The numerical accuracy studies do not state if the used numerical method computes the correct results or not. To do so, the results have to be compared to measured or computed data. In Paper 1, the computed results were compared to measured data for the flow in a single bent pipe. The measurements were performed by Sudo *et al.* (1998), and the same geometry and bulk velocity was used in the computations. Three different turbulence models were tested, a  $k - \epsilon$ -*RNG* RANS turbulence model, Smagorinsky LES turbulence model and Implicit LES and the results show that the Implicit LES gave the best agreement with measured data, see Figure 5.3.

Since no measurements of the flow field for the used turbine were available, the computed performance for the turbine was compared to data that was reported in the turbine map from the supplier for the actual turbine, c.f. Paper 2. Keeping in mind the used wall boundary conditions, the uncertainty of the inlet conditions and the numerical uncertainty, the results show fairly good agreement. In Paper 2 different causes for the differences in the results are discussed.

The used code have also been used to investigate the performance and the flow field in turbines by Palfreyman & Martinez-Botas (2005), who investigated

the flow field in a medium sized mixed flow turbocharger turbine for a pulsating operating condition. The unsteady RANS computations with the Sliding Mesh technique were compared to experimental data and flow field measurements by Laser Doppler Velocimetry (LDV). They concluded that the agreement for both cycle averaged and instantaneous data was reasonable, but there remained some uncertainty over the used inlet conditions. Palfreyman *et al.* (2002) used the same code with a *RNG*  $k$ - $\epsilon$  turbulence model to compute the non-pulsatile flow field in a mixed flow turbine. They concluded that the computed flow field agreed well with measured LDV data at the turbine exit. The turbine efficiency also agrees well with measured efficiency over the test range.

All this together show that the CFD code can be used to predict the performance of the turbine and that the code predicts the time resolved three-dimensional flow field in a reasonable way.

## CHAPTER 5

### Results

In this chapter, the most important and interesting results from the performed studies will be discussed. To start with, the results from the pipe flow study are presented, followed by the results from the investigation of the unsteady flow into a radial turbine of a turbocharger.

#### 5.1. Non-pulsatile and pulsatile flow in curved pipes

Two different geometries have been used in this study, see Figure 5.1. One geometry is similar to a runner on an exhaust manifold and the results from the investigation are used to get proper inlet conditions to the computations for the radial turbine. The results from the used code have also been compared to the measured data from the experiments performed by Sudo *et al.* (1998). When verifying computations against measured data, it is always hard to know if the used inlet conditions are the same as in the experiment. For example, the decay of vortices and swirl in pipes is slow, which has been showed in different studies, see for example Anwer & Lai (1989), Mattingly & Yeh (1991), Steenbergen & Voskamp (1998) and Najafi *et al.* (2005). Therefore, an investigation of the influence of the inlet conditions on the flow field has also been carried out.

##### 5.1.1. Method and computed cases

The Navier-Stokes equations have been solved numerically and different turbulence modeling approaches have been considered; the RANS and the LES approach. In the RANS computations, the  $k$ - $\epsilon$  *RNG* turbulence model has been used. The second order MARS scheme has been used for spatial discretization of the non-linear terms. Euler implicit temporal discretization is employed for integration of the momentum equations in time. The pressure is updated in each time-step, through the PISO procedure.

For the LES computations, two different subgrid scale modelling approaches have been used; the Smagorinsky model and Implicit LES. Different spatial discretization schemes have been tested, where the central difference scheme gives oscillations. Even a blended central difference scheme introduced wiggles. The

MARS scheme is the second order scheme that gives a solution without non-physical oscillations. A blended Crank-Nicholson scheme has been used for temporal discretization.

The computational domain for the single bent pipe consists of three parts, a straight section, a bend section and a second straight section, see Figure 5.1. The pipe diameter is 104 mm and the bend has a curvature radius of 208 mm, which gives a radius ratio of 4. The first section has a length of 14.5 diameters and the second straight section has a length of 12.5 diameters. For this case, a constant turbulent velocity profile is applied at the inlet.

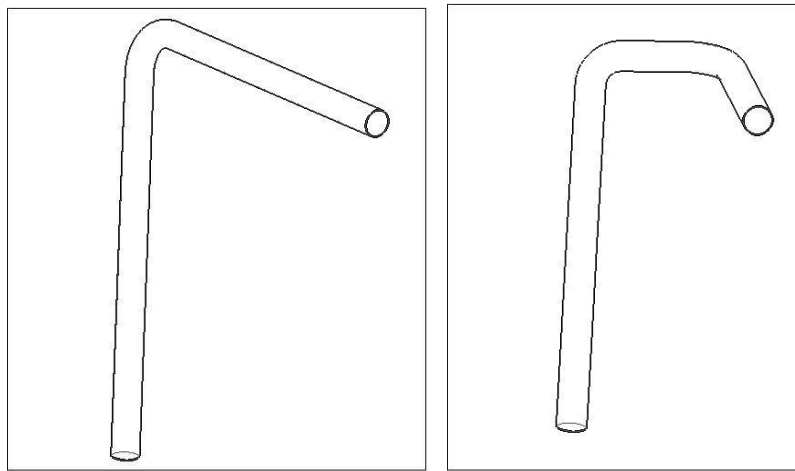


FIGURE 5.1. Computation domains.

The diameter for the double bent pipe is 10 mm. The pipe has two bends with radius  $r_1=10$  mm and  $r_2=15$  mm, respectively. The inlet section is 12 diameters long, the section between the two bends is 2.5 diameters long and the outlet section is 6 diameters long. This pipe has a similar shape as one of the runners of an exhaust manifold found on a turbocharged IC-engine. At the pipe inlet, a time resolved mass flow pulse and temperature are specified and at the outlet a constant pressure is applied. The walls are modelled as being smooth and adiabatic. The time averaged bulk velocity is 110 m/s, which corresponds to a Reynolds number of 8900. The frequency is 50 Hz which gives a Womersley number of 8. The maximal velocity is 250 m/s, which corresponds to a Reynolds number of 20 200.

5.1.2. *Non-pulsatile flow in a single bent pipe*

The time mean flow obtained from the LES computations shows that the Dean vortices are created at  $\varphi \approx 30^\circ$ , which is at the same location as reported in the experiment performed by Sudo *et al.* (1998). At the exit of the bend, the time mean secondary flow consists of the counter-rotating Dean vortices with the centres located in the lower part of the pipe, as shown in Figure 5.2. The axial velocity has a C-shaped distribution in the cross-stream plane, with its maximum at the outer part of the bend. The Dean vortices dominate the secondary flow at the region downstream of the bend and the vortex cores are moving up against the centre of the pipe when they are convected downstream. 10 pipe diameters downstream of the bend, the vortices have almost dissipated and the axial velocity distribution is still C-shaped at this location. The instantaneous secondary flow at the exit plane of the bend is not symmetric and at certain instants up to 6 vortices, where two of them are counter-rotating with respect to the Dean vortices, is observed. The vortices are meandering in the cross-stream plane and the C-shaped axial velocity contour is meandering from one side of the pipe to the other side and the Dean vortices at each side move up and down with varying strength. The axial velocity and the location of the Dean vortices is varying with a Strouhal number of approximately 2, where the Strouhal number here is based on the bulk velocity and the pipe radius.

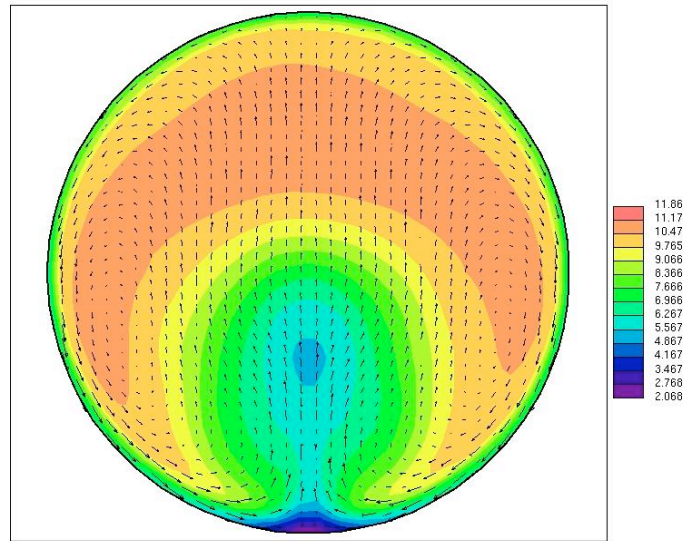


FIGURE 5.2. The counter-rotating Dean vortices at the outlet of the bend. Contour: axial velocity component, vector: In-plane velocity components.

The comparison of the computed velocity profiles with the measured profiles has been conducted at 3 different locations; half a diameter upstream of the bend, at the exit of the bend and half a diameter downstream of the bend. Half a diameter upstream of the bend, the deviations between the computed and measured velocity profiles are smaller than the measurement error. At the evaluation stations downstream the bend, the deviation is larger and the RANS computation could not capture the behaviour of the flow field, especially at the inner wall, where the computed streamwise velocity is lower for all cases than it is in the measurement, see Figure 5.3. The time mean velocity profiles from the LES computation without a subgrid scale model gives better agreement with the measured velocity profiles at all evaluation stations, but the LES computations over-predict the axial velocity at the outer part of the bend and under-predict the velocity in the centre part of the cross-section of the bend.

Despite the fact that the results from the RANS method give the largest deviation from the measured velocities, this model is used to investigate the effects of perturbations at the inlet. The reason is the long computation times that are required for the LES approach. Different inlet velocity profiles are applied at the inlet to the single bend pipe. The imposed eccentricity and swirl are used to assess the sensitivity of the results to inlet perturbations. These types of perturbations are often found in experiments where the inlet pipe is short and no fully developed turbulent pipe flow can develop. When comparing the velocity profiles for the different cases with measured velocity profiles, it is clear that the case with the swirling motion gives the best agreement at the exit of the bend. One way to give a measure of the inlet effects is to compare the Root Mean Square (RMS) value of the  $\partial U/\partial \zeta$ , where  $\partial U$  is the difference between the velocity profile obtained with a symmetric velocity profile and a non-symmetric or swirling velocity profile at a certain station.  $\partial \zeta$  is the difference in kinetic energy at the inlet for the symmetric inlet profile and a non-symmetric or swirling inlet profile. Table 1 shows the results from the analysis at the exit of the bend and it is clear that inlet condition with swirling flow gives the largest effect. In this case the flow field is rotated due to the swirling motion before the bend and hence, the low velocity region is turned a few degrees in the clockwise direction. This is also the inlet profile which gives the best agreement with the measured velocity profiles downstream of the bend, indicate that there is probably a swirling secondary flow component in the experimental case too.

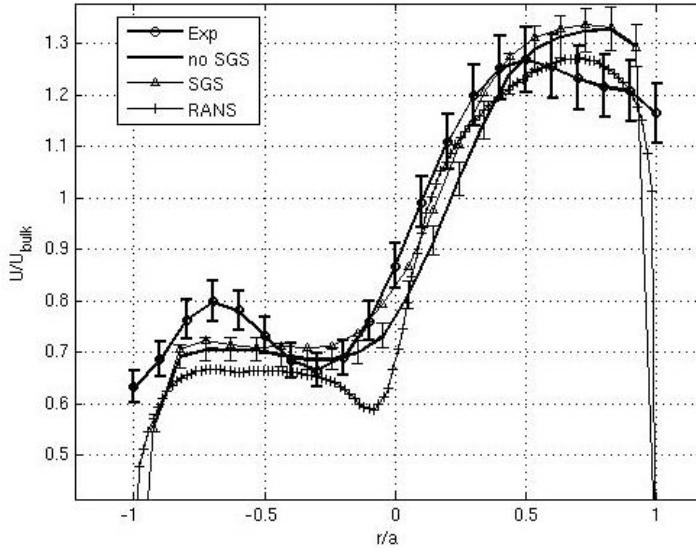


FIGURE 5.3. Result from RANS and LES computations. Streamwise component half a diameter downstream of the bend.

TABLE 1. RMS value of  $\partial U/\partial \zeta$  at the exit of the bend.

Inlet profile	Eccentric 1	Eccentric 2	Eccentric 3	Swirl
RMS ( $\partial U/\partial \epsilon$ )	0.093	0.046	0.16	0.55

### 5.1.3. Pulsatile flow in a double bent pipe

The pulsatile flow in the double bent pipe has been computed with both the RANS and the LES approach. In this section, the results from the LES computations are presented.

During the acceleration phase of the inlet velocity, the Dean vortices are created in the first bend. At the outer part of the entrance to the first bend a recirculation zone is located during the whole pulse period, except when flow reversal occurs. The recirculation is an effect of the adverse pressure gradient in the streamwise direction at the outer wall. At the entrance to the second bend, the maximum velocity region is located at the inner wall, which means that the region of maximum velocity is rotated  $90^\circ$  from the exit of the first bend. The secondary flow downstream of the second bend is dominated by a swirling motion and the Dean vortices formed in the second bend. One of the Dean

vortices from the first bend interacts with the swirling motion, while the other has been dissipated. Further downstream, the strength of the Dean vortices from the second bend are decaying, but they still have an influence on the main secondary swirling motion, which is not symmetric, as shown in Figure 5.4. The figure depicts the isosurface of the vortices using the  $\lambda_2$  criterion for defining a vortex (Jeong & Hussain (1995)). The location of the centre of the swirling motion is not stationary in the cross-stream plane during one pulse and the strength of the swirling motion at the outlet varies with the amplitude of the axial flow. During the last part of the deceleration phase at the inlet, flow reversal occurs in the boundary layer at walls of the pipe, while the flow in the centre part of the pipe is not reversed, as shown in Figure 5.5.

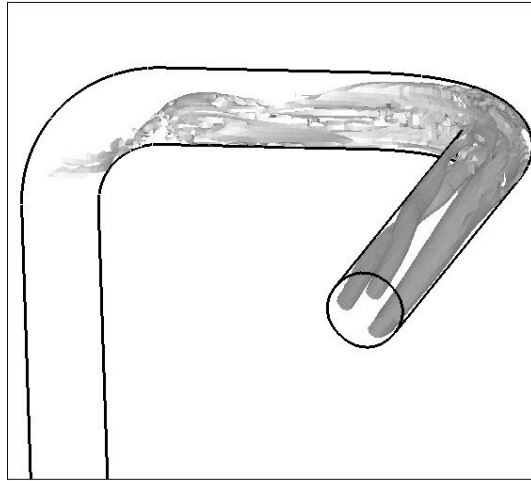


FIGURE 5.4.  $\lambda_2$  showing the different structures in the pipe.

As mentioned above, pulsating flow gives a phase shift between the bulk flow and the pressure. The phase shift is not constant during the pulse period. For the LES computation the corresponding range of phase lag is between  $19^\circ$  and  $52^\circ$ . The maximum phase shift occurs when the inlet flow changes direction, and the minimum phase shift occurs when the mass flow reaches its maximum at the inlet. At minimum phase shift, the turbulent energy is much higher than it is when maximum phase shift occurs, which is in agreement with the conclusions by Ramaprian & Tu (1983).

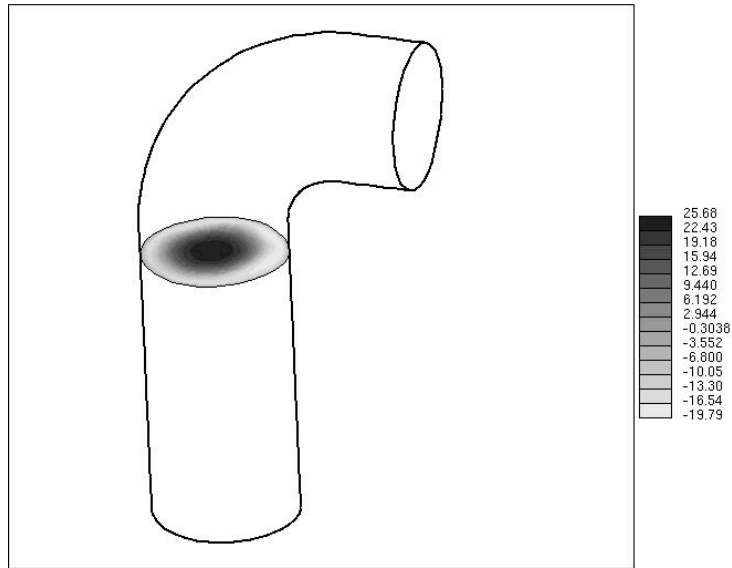


FIGURE 5.5. Instantaneous axial velocity component, showing the effect of pulsating flow with reversed flow near the wall.

## 5.2. Unsteady flow in a radial turbine

### 5.2.1. Method and geometry

For the turbines computations, the ILES approach has been used. This approach is much more computationally expensive as compared with RANS approach. However, the most energetic turbulent scales are resolved and thereby one gets more information about the unsteady flow in the turbine. It also enables one to use Proper Orthogonal Decomposition (POD) of the time-resolved flow field. The results from the POD can be used when developing a low order model for the turbine. The results from the LES computations can also be used to extract the acoustical source terms that can be used to compute the noise generation in the turbine. As in the pipe cases, the second order MARS scheme has been used for spatial discretization of the convection terms. For the temporal discretization the first order implicit Euler scheme has been employed. The pressure has been updated using the PISO algorithm at each time-step. The wheel is modelled by the sliding mesh technique, which implies that the mesh which represents the turbine wheel is rotating relative to the stationary turbine house. The total number of cells is 1 111 720 and the cell distribution and averaged cell size at the different parts of the grid is given in Table 2. The averaged cell size is defined as the cubic root of the ratio between the volume

and the number of cells for each region. In the rotor region, only hexahedron cells have been used, while in the rest of the domain an unstructured grid has been used with 95% hexahedron cells.

TABLE 2. Grid resolution.

	Number of cells	Averaged cell size (mm)
Volute	275 084	0.77
Wheel	297 648	0.42
Diffuser	538 988	0.71
Complete turbine	1 111 720	0.69

The turbine under consideration is a commercially available turbine with a size that is typical for a turbocharger mounted on a 2.0 litre IC engine of a passenger car. The turbine is a nozzle-less, 9 bladed radial turbine with the waste-gate valve closed. The complete turbine and the turbine wheel are shown in Figure 5.6. The leading edge tip radius of the wheel is 22.10 mm and the trailing edge tip radius is 18.75 mm.

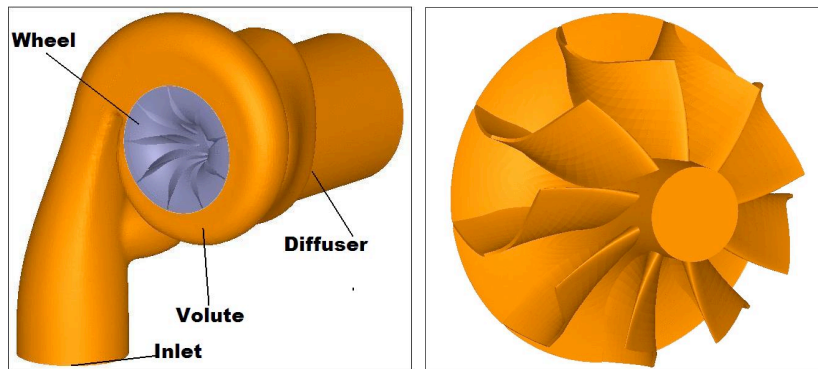


FIGURE 5.6. The complete turbine geometry and the wheel.

The time-step for the non-pulsatile computations is  $10^{-6}$  seconds which corresponds to a rotation of the wheel of  $0.6^\circ$ /iteration. For the pulsatile computations, the time-step is  $4 \cdot 10^{-7}$  seconds.

## 5.2.2. Pulsatile flow in turbocharger

Three different cases have been computed, where Case 1 has a frequency, mass flow and temperature corresponding to an engine working with wide open throttle at a speed of 1500 rpm, see Figure 5.7. The rotational speed of the turbine is 97 897 rpm. Case 2 has the same mass flow and temperature profile as for Case 1, but the frequency of the pulsations is ten times higher. This is not a realistic case for a turbocharger of a passenger car, but this case is used to investigate the effects of a higher frequency of the pulsatile inlet conditions. For Case 3, the inlet conditions and the rotational speed of the turbine corresponds to an IC-engine working at 3000 rpm. The inlet conditions are shown in Figure 5.7. The rotational speed of the turbine for this case is 150 000 rpm. At the outlet, a minimal reflecting pressure condition is applied to ensure that no reflected pressure waves contaminate the numerical solution.

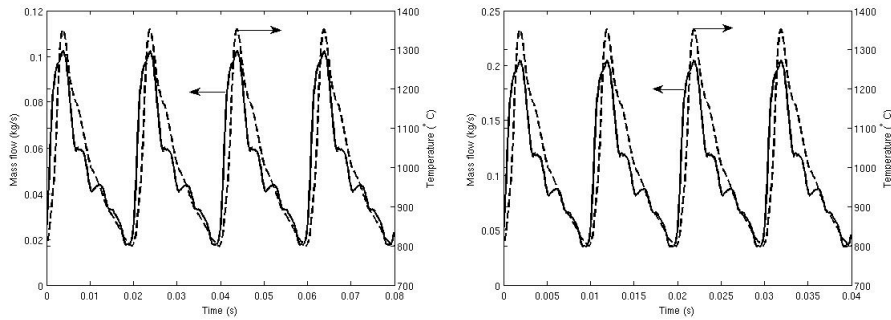


FIGURE 5.7. Specified mass flow and temperature at the inlet to the turbine for Case 1 (left) and Case 3 (right), respectively.

The shaft power varies during the pulse, as shown in Figure 5.8. As can be seen, the shaft power is higher when the mass flow at the inlet is decreasing. The isentropic efficiency,  $\eta_{is}$  also varies during the pulse. At certain times the nominal efficiency is negative since at these instances the shaft torque is itself negative due to a fixed rotational speed of the turbine wheel. The same behaviour for a mixed flow turbine at pulsatile flow conditions at the inlet was reported by Palfreyman & Martinez-Botas (2005) who conducted both numerical computations and experiments to investigate the performance of mixed flow turbine working under pulsatile flow conditions. As also can be seen in plots of the shaft power, an oscillation with a frequency corresponding to the blade passage is superimposed on the shaft power. The local minimum of the shaft torque occurs when the blade passes the tongue which gives a disturbance of the pressure distribution on the blade, resulting in a disturbance of the shaft torque.

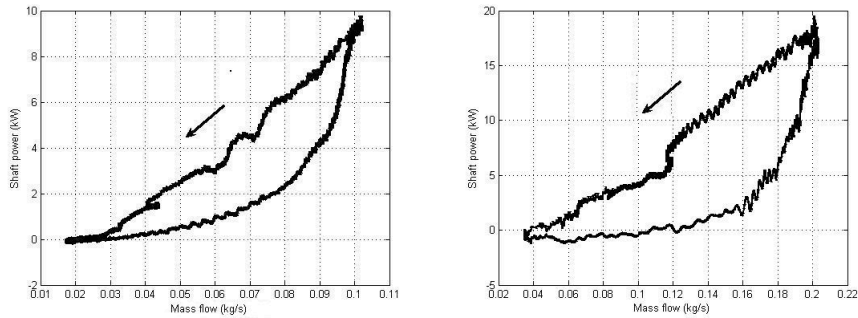


FIGURE 5.8. Computed shaft power vs. mass flow at inlet for Case 1 (left) and Case 3 (right), respectively.

The flow field has only been investigated in detail for Case 1 and Case 3, since the conditions of Case 2 is not encountered in engines for passenger cars. The major difference between the flow fields in the volute for Case 1 and Case 2, is that Case 2 has higher velocity in the volute due to the phase shift between pressure and mass flow. The higher velocity in the volute for Case 2 implies that the inlet angle to the turbine wheel is different, which gives incidence losses, and hence, affects the shaft power in a negative way.

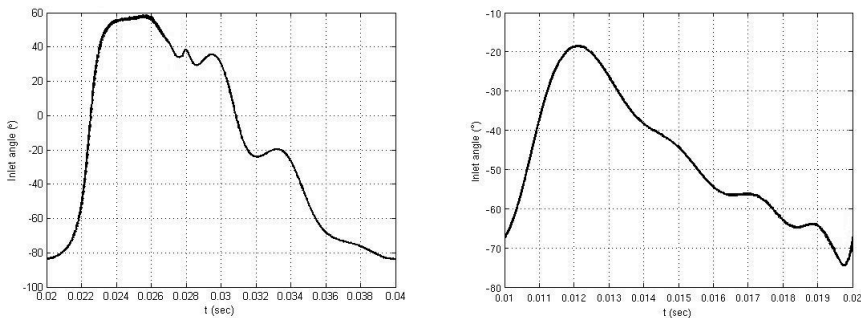


FIGURE 5.9. Relative incidence angle to the wheel for  $90^\circ$  azimuthal angle during one pulse. Case 1 to the left, Case 3 to right.

The incidence angle to the wheel varies during the pulse, due to the varying mass flow at the inlet. In Figure 5.9, the relative inlet angle for  $90^\circ$  azimuthal angle is plotted for Case 1 and Case 3. As can be seen, the inlet angle for Case 1 varies from approximately  $-85^\circ$  to  $60^\circ$ . For Case 3, the inlet angle varies from approximately  $-67^\circ$  to  $-25^\circ$ , which is more favourable. For Case

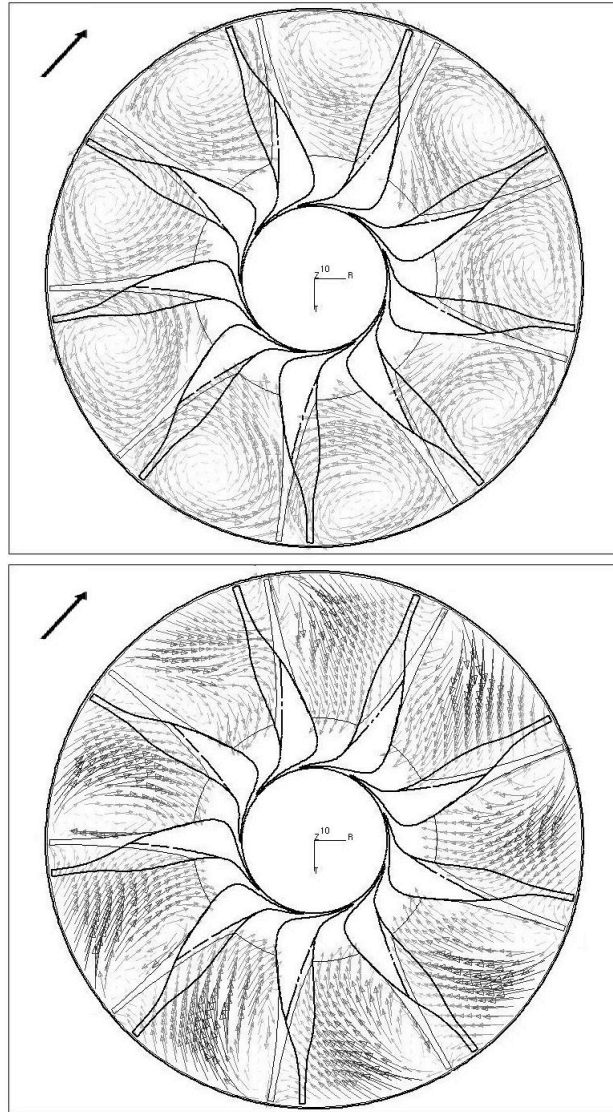


FIGURE 5.10. Snapshot of the in-plane relative velocity field at the inlet plane to the wheel, Case 1. The arrow shows the direction of rotation. The top figure shows the flow field with low mass flow through the turbine. The bottom figure shows the flow field when the mass flow through the turbine is high.

1 only a small phase shift occurs between the mass flow and the pressure at the inlet. The shaft torque is also almost in phase with the mass flow and pressure at the inlet, and hence a time resolved isentropic efficiency can be defined. When the frequency increases, the phase shift is significant. This implies that an isentropic efficiency can not be computed in an accurate way. For Case 1, the maximum phase shift between the mass flow and the pressure is approximately  $20^\circ$  which occurs when the mass flow into the domain is low. When the mass flow reaches its peak, the phase shift is below  $4^\circ$ . For Case 3, the phase shift between the mass flow pulse and pressure at the inlet when maximum mass flow occurs is approximately  $20^\circ$ , which is significantly higher than for Case 1. This implies that the quasi-stationary assumption is not valid for a turbine working in pulsatile flow. The deviation from the quasi-stationary assumption also depends on that the flow separation from the turbine wheel blades is more severe during the acceleration phase as compared to the same mass flow during the deceleration phase. The deviation from the quasi-stationary approach increases with increasing frequency, which has also been reported by Wallace & Blair (1965). When the mass flow through the

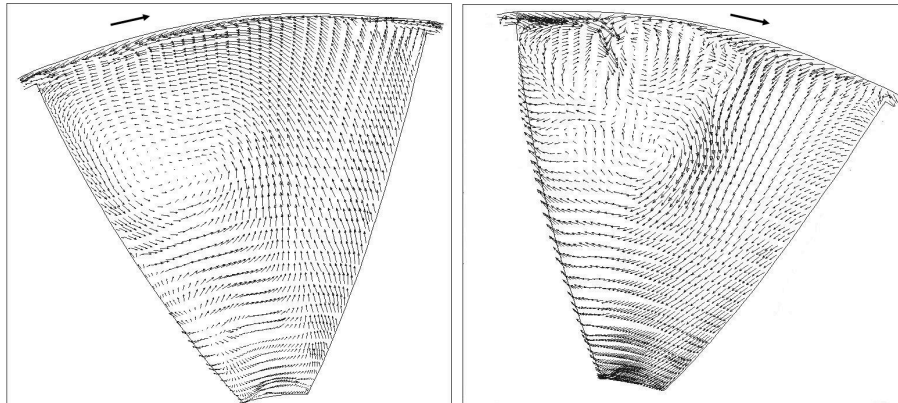


FIGURE 5.11. Snapshot of the in-plane relative velocity at a plane between the leading and trailing edge of the wheel, Case 1. The left figure shows the flow field with low mass flow through the turbine. The right figure shows the flow field when the mass flow through the turbine is high.

turbine is low, the relative inlet angle is below  $-40^\circ$ . This implies that the pressure is higher at the suction side of the blade tip at the leading edge, which drives the flow over the tip from the suction side towards the pressure side. This leads also to the role-up of the tip vortex at the pressure side, as shown in Figure 5.10. When the mass flow increases during the pulse, the inlet angle

increases and flow separation occurs at the suction side of the blade. The vortex due to separation is much stronger than the tip vortex formed at the pressure side of the blade. The tip vortex formed at the leading edge detaches and is convected downstream between the blades. Downstream between the blades, the secondary flow at high mass flow contains three different structures; the detached tip vortex from the leading edge that is convected downstream, the tip vortex that is created between the blade tip and the shroud and a vortex that is counter-rotating as compared to the tip vortices, as depicted in Figure 5.11. Between the blades, the pressure gradient drives the flow in the boundary-layer at the shroud from the pressure side towards the suction side. When the flow in the boundary-layer at the shroud is affected by the strong jet that is formed at the tip, it is deflected inwards between the blades and a vortex starts to roll up. The higher mass flow at the inlet for Case 3 implies that the Mach number

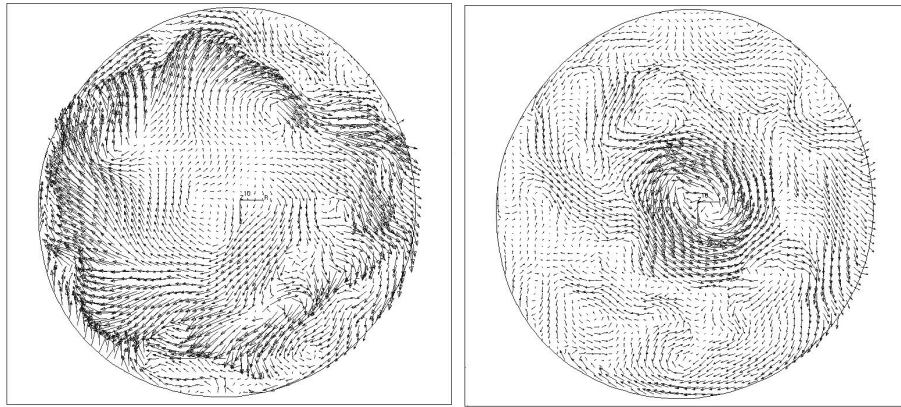


FIGURE 5.12. Snapshot of the velocity field in the diffuser, half a wheel diameter downstream of the trailing edge of the wheel, Case 1. The left figure shows the flow field with low mass flow through the turbine. The right figure shows the flow field when the mass flow through the turbine is high.

is higher. When the mass flow through the wheel reaches its maximum, a shock wave is formed between the leading edge of the blade and the wall at the tongue. The shock disturbs the flow, and the tip vortex at the suction side at the leading edge where the shock occurs is very strong. Since the interval when supersonic flow occurs in the volute only corresponded to a few blade passages, it does not deteriorate the shaft torque. The higher mass flow for Case 3 also results in a stronger pressure gradient between the blades which gives a higher power output. Despite the stronger pressure gradient, the tip vortices for Case

3 are not as strong as for Case 1, depending on a more optimal inlet flow angle into the wheel.

Downstream of the wheel, the centre line vortex has the direction of rotation opposite to direction of the rotation of the wheel when the mass flow through the turbine is high. For Case 3, this vortex is weaker as compared to the centre line vortex for Case 1, due to a more favourable flow outlet angle for Case 3. When the mass flow is low for both cases, no coherent structures are observed at the centre-line down-stream of the wheel, as shown Figure 5.12.

### 5.2.3. Effects of inlet perturbations

The effect of different perturbations at the inlet on the performance of a radial nozzle-less turbine has been assessed. Five different inlet conditions have been considered. These are given in Table 3. For all cases, a turbulent velocity profile and the temperature are specified at the inlet boundary and different perturbations are added to this velocity profile. The mass flow at the inlet to the turbine has been kept constant (equal to 0.08144 kg/s) by varying the velocity. The temperature at the inlet has been set to 1000°C for all cases. At the outlet, a non-reflective boundary condition is applied. The walls are assumed to be smooth and adiabatic.

TABLE 3. Computed cases.

Case	Turbulence intensity	Secondary flow	Strength of secondary flow
1	0%	-	-
2	5%	-	-
3	5%	Dean	0.10
4	5%	Swirl	0.28
5	5%	Swirl	1.5

In Figure 5.13 the axial and azimuthal velocity components at the inlet to the turbine are plotted for the different cases. For Case 1, no perturbations are added. Case 2 had an inlet profile with turbulent fluctuations. The turbulence intensity for Cases 2-5 is 5% and the turbulent fluctuations at the inlet boundary are created by the method proposed by Klein *et al.* (2003). Case 3 has both turbulent fluctuations and secondary flow in the velocity profile, where the secondary flow consists of a pair of counter-rotating Dean vortices, see Figure 5.14. Cases 4 and 5 have, in addition to the turbulent fluctuations, a swirling motion added, where Case 5 has the stronger swirl. The strength of the swirl at the inlet is defined as the azimuthal velocity at the edge of the inlet

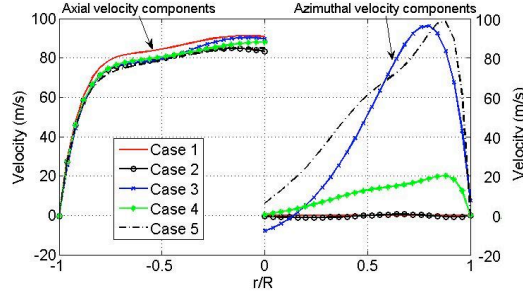


FIGURE 5.13. Axial and secondary velocity components at the inlet.

boundary divided by the axial bulk velocity. The strength of the Dean vortices is defined as the area averaged value of the secondary component divided by the axial component at the inlet. The strength of the secondary flow is obtained from LES-computations of the pulsatile flow in a four to one exhaust manifold.

The evaluated data has been gathered for the last 4 of 20 revolutions of the turbine. This corresponds to 36 blade passages. This data have been used for the computing the time averages of the different parameters. In Figure 5.15

TABLE 4. Shaft power, available power at the inlet, isentropic efficiency, utility factor and pressure ratio.

Case	$P_{SHAFT}$ (kW)	$P_{INLET}$ (kW)	$\eta_{is}$	$\kappa$	PR
1	5.02	82.18	0.66	0.061	1.41
2	4.34	82.14	0.66	0.053	1.34
3	4.41	82.26	0.64	0.054	1.36
4	4.40	82.12	0.66	0.053	1.35
5	4.05	82.35	0.64	0.048	1.32

the time resolved shaft power for the different cases is shown. The shaft power fluctuates with a frequency that corresponds to the blade passage frequency. Fluctuations with lower frequencies are also present for all cases, depending on flow unsteadiness in the volute. In Table 4 the time averaged shaft power and two different ways of expressing the efficiency are given. For the time mean value of the shaft power, there are differences between the cases. The time mean shaft power for Case 5 is 19% lower than for Case 1, which is greater than the estimated numerical uncertainty. For Cases 2-4, the differences in the shaft power as compared to Cases 1 or 5 are of the same order as the numerical

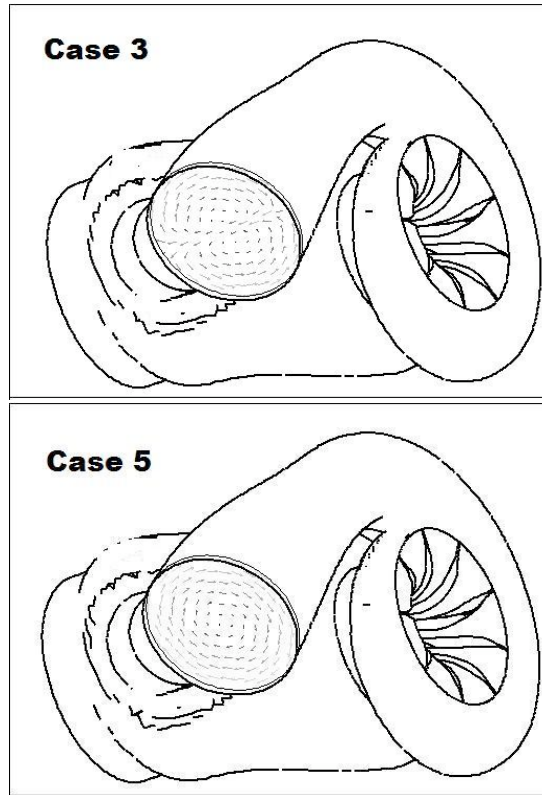


FIGURE 5.14. The secondary flow at the inlet plane for Case 3 and 5, respectively.

uncertainty. Altogether, the computations show that different perturbations at the inlet do affect the performance of the turbine. As can be seen in Table 4, the isentropic efficiency does not reflect the fact that the shaft power is almost 20% lower for Case 5 as compared to Case 1. This is so since the isentropic efficiency also takes into account the energy content of the flow after the turbine, which can be used to drive a second turbo-charger. A better definition of the efficiency is the utility factor,  $\kappa$ . The utility factor is defined as:

$$\kappa = \frac{P_{SHAFT}}{P_{INLET}} \quad (5.1)$$

This better reflect the effects of the perturbation at the inlet. In this definition,  $P_{INLET}$  is the available power at the inlet boundary, defined as:

$$P_{INLET} = \int_{Inlet} \left( \frac{1}{2} \cdot u_i \cdot u_i + h \right) \rho U_n dA \quad (5.2)$$

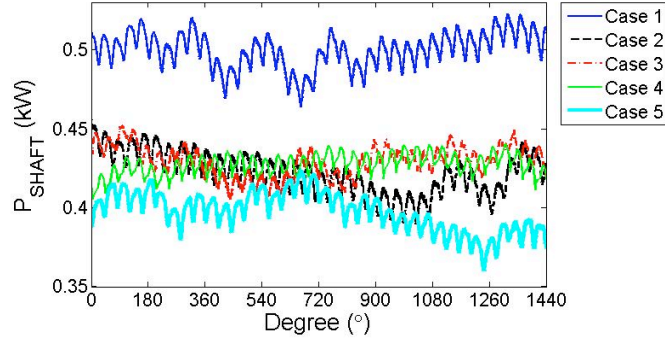


FIGURE 5.15. The time resolved shaft power for the different cases during 3 turbine wheel revolutions.

where the velocity  $u_i$ , density  $\rho$  and the enthalpy  $h$  is at the inlet boundary.  $U_n$  is the normal velocity component. The utility factor can also be viewed as an efficiency parameter which reflects the ability of the turbine to extract power from the provided power. A result from the different perturbations at the inlet is that the axial inlet velocity component is different for the different cases, as seen Figure 5.13. This is so due to different absolute pressure at the inlet. Although Case 1 has the largest pressure ratio over the turbine it has the lowest absolute pressure at the inlet and the outlet, since the turbine extracts most energy from the gas for this case. The lowest pressure for Case 1 results in the highest perpendicular velocity at the inlet, and hence, the highest velocity in the volute. This results in the highest velocity into the turbine wheel, as seen Figure 5.16. For all the cases, a coherent structure is created at the inlet to the waste gate channel and it is convected downstream. For Cases 1-4 the vortex from the waste gate channel interacts with the wake downstream of the tongue. For Case 5 the vortex that is created at the inlet to waste gate channel does not interact with the wake downstream of tongue since it is convected downstream at the side of the tongue, as seen in Figure 5.17. In the volute, the strength of this vortex increases due to the radial pressure gradient. These two counter-rotating vortices, shown in Figure 5.18, are meandering in the cross-stream plane which create a non-uniform velocity distribution into the turbine wheel in space and time.

The highly swirling motion at the inlet also feeds the wake behind the tongue. This effect can be seen in the energy spectra at a location just downstream of the tongue. Case 3 has the highest fluctuating energy at a point downstream of the tongue, whereas Case 1 has there the lowest fluctuation energy.

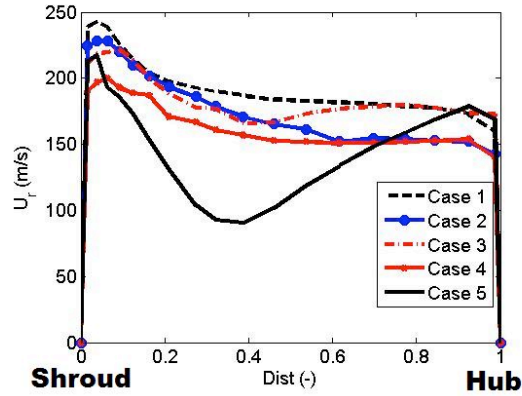


FIGURE 5.16. The radial velocity component for the different cases at the inlet to wheel at a location that corresponds to an azimuthal angle of  $90^\circ$ . Positive velocity is defined as being directed inwards.

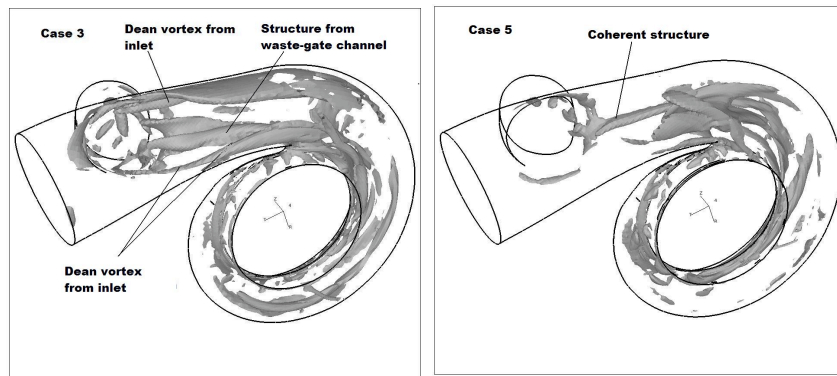


FIGURE 5.17.  $\lambda_2$  for Case 3 (left) and Case 5 (right), showing the coherent structures created at the inlet to waste-gate channel.

The non-uniform and in time varying axial velocity distribution in between the blades affects the pressure distribution at the blades. In Figure 5.19 the instantaneous pressure coefficients  $C_p$  are plotted for both the suction and the pressure side of a blade for the five cases along the chord between the tip and the hub.  $C_p$  is computed for the same blade and the phase angle for the different cases. Case 1 has the best pressure distribution. This is also the case with the highest axial velocity in between the blades. Case 5 has the lowest axial

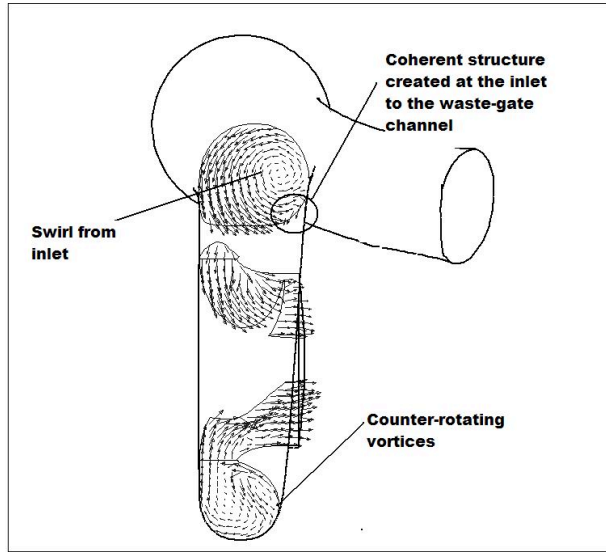


FIGURE 5.18. In-plane velocity components for Case 5, showing the coherent structure created at the inlet to waste-gate channel.

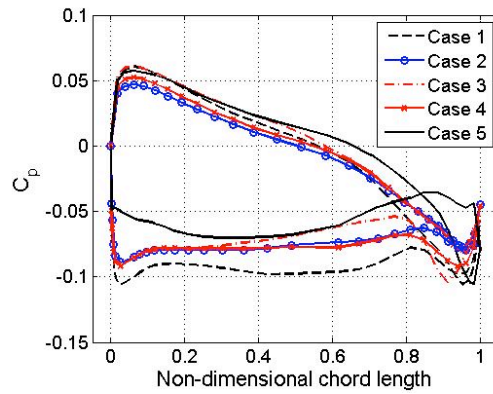


FIGURE 5.19. The instantaneous pressure coefficient along the chord of a blade at the pressure and suction side.

velocity in between the blades, which is also reflected in  $C_p$ . Since the flow for all cases is unsteady, the pressure distribution varies depending on where the blade is located during the revolution. The largest differences among the

different cases are on the suction side, since this blade side is the most sensitive to changes of the relative incidence angle.

The highest velocity for Case 1 in between the blades implies that this case has the strongest azimuthal pressure gradient. This results in the strongest tip vortices at the leading edge of the blades. Case 5, which has the lowest velocity in between the blades, has the weakest tip vortices. The secondary flow structures in between the blades seem to have a secondary effect on the shaft power output.

## CHAPTER 6

### Conclusions

The unsteady flow in pipes and a radial turbine have been computed using LES. The purpose of the pipe flow computations was to study the non-pulsatile and pulsatile internal flow in curved geometries, which are relevant to the inlet to the turbo-charger turbine. For one of the used geometries, a comparison with measured data has also been performed. The results show that an Implicit LES turbulence modelling approach gives the best agreement with measured velocities among the tested turbulence modelling approaches. For the pulsatile flow a phase shift between the pressure and the bulk flow has been found. The phase shift varies during the pulse, depending on the balance between the different terms in the momentum equation. The phase shift also implies that flow in the boundary layer and in the core region of the pipe are out phase, since the low momentum flow in the boundary layer is more sensitive to changes in the axial pressure gradient than the flow in the core region. This results in an increased mixing in the region near the wall resulting in higher heat transfer to the walls.

The bends in the pipe introduced secondary flow structures. In the first bend, two counter-rotating vortices are created and the axial velocity component after the bend is not uniformly distributed. When this non-uniform axial velocity distribution enters a second bend, situated in an orthogonal plane downstream of the first bend, a swirling motion is created downstream of the second bend. This swirling motion is also affected by the Dean vortices created in the bends upstream. Since an exhaust manifold can be viewed as being composed of straight and bent pipe sections, the flow into the turbine has non-negligible secondary flow structures in addition to the pulsatile axial flow. The pulsatile flow in the turbine also increases the heat losses. This all together implies that a turbocharger turbine for an IC-engine will have operation conditions that are far away from the conditions that they are designed and tested for.

The effect of the pulsatile flow on the turbine performance has been assessed by conducting computation at different frequencies and mass flows. The major conclusions of that study are as follows:

- The turbine cannot be treated as being quasi-stationary when working in pulsatile flow, due to inertia of the system, detached flow during the acceleration phase and a non-constant phase shift between the pressure, mass flow and shaft power. The deviation from the quasi-stationary approach increases with increasing pulsation frequency. These factors affect the accuracy of the results from 1-D models that are based on turbine maps that are measured under steady-state flow conditions.
- For the two cases with the same mass flow amplitude, but different frequencies of the pulsations, the peak shaft power is 4 % lower for the case with the highest frequency. This is due to an unfavourable incidence angle of the flow into the wheel, since the velocity in the volute is higher for this case depending on a lower pressure ratio over the turbine and larger phase-shift between the pressure and mass flow. During the deceleration phase, the incidence angle is more favourable for the case with higher frequency, resulting in a temporary higher power output.
- The incidence angle of the flow into the wheel has large variation during the pulse which affects the efficiency of the turbine. A deviation from the optimal angle results in strong tip vortex at the leading edge of the blade, which detaches and is convected downstream and affecting the axial velocity in between the blades.

To investigate the effects on the turbine performance due to secondary flow structures created in manifold upstream of the turbine, computations with different types of perturbations at the inflow to the turbine have been carried out. The results show that both small and large scale perturbations at the inlet to the turbine affect the shaft power. The undisturbed inlet profile gives the best power output from the turbine while a case with strong swirl in combination with 3-dimensional turbulent perturbations gives the largest loss in the shaft power output. The deterioration of the performance is due to large scale structures created in the volute, which then result in unfavourable inlet conditions into the wheel. Another interesting result is that the case with the highest shaft power and the largest pressure ratio has the lowest absolute pressure at the turbine inlet, which is beneficial, since it decreases the pump-losses of the internal combustion engine.

### 6.1. Future work

The work related to the turbine so far has been limited to a single case on a single grid resolution. For assessing the quality of the results one has to repeat the computations also on refined grid. One would like to improve the resolution of the tip area as well as the near wall regions. One may expect that the lack of near wall resolution on the blade may lead to under-estimation

of the separation regions and thereby also some viscous losses. One may also expect that the separation bubbles are unsteady and this may interact and induce further unsteadiness in the turbine. The underlying physics of such effects have to be further explored. Additionally, the effects of losses through the turbine housing have been neglected due to the use of adiabatic conditions.

One of the objectives of this work has been to better understand the dynamics of the flow in the turbine. This is expected to be done by utilizing Proper Orthogonal Decomposition (POD) that is an optimal expansion in orthogonal functions. The expansion is optimal in the sense that the kinetic energy of the flow can be expressed in minimal number of terms. We intend also to use such POD expansion to define a lower dimensional dynamical system. This is to be derived by applying a Galerkin projection of the POD expansion on the governing equations. Such approach can be as efficient for simulation as current 1-D tools but shall take into account the inherent 3-D characteristics of the flow.

## CHAPTER 7

### Papers and authors contributions

#### **Paper 1**

*Numerical computations of steady and unsteady flow in bended pipes.*

F. Hellstrom & L. Fuchs.

*AIAA 2007-4350, 37th Fluid Dynamics Conference and Exhibit, Miami Fl. 2007*

The purpose of this work is to investigate the non-pulsatile and pulsatile flow in bent pipes. The results from one of the cases with different turbulence modelling approaches are compared with measured data. A study of the influence of perturbations at the inlet is also performed. The work was performed by Hellstrom under supervision by Prof. Fuchs. The results were presented at the 37th Fluid Dynamics Conference and Exhibit, Miami, Florida, 2007 by Hellstrom.

#### **Paper 2**

*Numerical computations of pulsatile flow in a turbo-charger.*

F. Hellstrom & L. Fuchs.

*AIAA-2008-735, 46th Aerospace Sciences Meeting, Reno, 2008.*

The objective of this work is to assess the effect of different pulsatile inlet conditions on the turbine performance. Therefore three different cases with different frequencies and mass flow pulses are considered. The performance of the turbine for the non-pulsatile computations is also compared with measured performance for the same geometry. The work was performed by Hellstrom under supervision by Prof. Fuchs. The results were presented at the 46th Aerospace Sciences Meeting, Reno, 2008 by Hellstrom.

### **Paper 3**

*Effects of inlet conditions on the turbine performance of a radial turbine.*

F. Hellstrom & L. Fuchs.

*Submitted to ASME Turbo Expo 2008: Power for Land, Sea and Air June 9-13, 2008, Berlin, Germany.*

In this paper the effect of the different perturbations on the performance of a radial nozzle-less turbine is assessed and quantified by using Large Eddy Simulations. Five different cases are considered, where the base case has a non-disturbed velocity profile applied at the inlet. The other cases has 3-dimensional turbulence added to the velocity profile. Three of the cases has also different secondary flow structures added at the inlet. The turbine performance is compared for the different cases and the flow field is investigated to give a better insight into the unsteady flow field and the effects from the different inlet conditions. The work was performed by Hellstrom under supervision by Prof. Fuchs. The paper is submitted to ASME Turbo Expo 2008: Power for Land, Sea and Air June 9-13, 2008, Berlin, Germany.



## Acknowledgements

First of all I would like to thank my supervisor Professor Laszlo Fuchs for all encouragement, support and guidance throughout this work.

I would also like to thank my employer GM Powertrain, Sweden AB, for making my PhD studies possible and I especially would like to thank my manager Dr. Reinmann, who gave me the possibility to conduct the PhD studies without any interruptions. Thanks also to Anna Svärd and Per Birkestad for commenting my manuscript.

The Swedish Emission Research Program is acknowledged for the financial support.

Last, but definitely not least, I would like to thank my wife and daughter for all the patience and love.

## References

- ANDERSEN, J., KARLSSON, E. & GAWELL, A. 2006 Variable turbine geometry on si engines. *SAE 2006 World Congress, Detroit, Michigan* **SAE 2006-01-0020**.
- ANWER, M. SO, R. M. C. & LAI, Y. G. 1989 Pertubation and recovery from bend curvature of a fully developd turbulent pipe flow. *Physics of Fluid* **1**, 1387–1397.
- ARCOUMANIS, C., KARAMANIS, N., MARTINEZ-BOTAS, R. & SU, C. C. 1999 Unsteady characteristics of a mixed-flow turbocharger turbine. *IMechE paper no C557/030* pp. 905–921.
- BAINES, C. N. 2005 Fundamentals of turbocharging. *Concepts NREC, ISBN 0-933283-14-8* .
- BARDINA, J., FERZIGER, J. & REYNOLDS, W. 1980 Improved subgrid scale models for large eddy simulation. *AIAA Paper 80-1357* .
- BARR, L., SPENCE, S. W. T., & McNALLY, T. 2006 A numerical study of the performance characteristics of a radial turbine with varying inlet blade angle. *ImechE Conference Transactions from 8th International Conference on Turbochargers and Turbocharging* pp. 169–181.
- BENSON, R. 1974 Nonsteady flow in turbocharger nozzleless radial gas turbine. *SAE 740739* pp. 1–11.
- BENSON, R. & SCRIMSHAW, K. 1965 An experimental investigation of non-steady flow in a radial gas turbine. *Instn Mech Engrs* **180**, 74–85.
- BRUCKER, C. 1998 A time-recording piv-study of the swirl switching effect in a 90° bend flow. *Proceedings of the Eight International Symposium on Flow Visualizations, Sorrento, Italy* .
- CAPOBIANCO, M. & GAMBAROTTA, A. 1990 Unsteady flow performance of turbocharger radial turbines. *C405/017, Proceeding of the Institute of Mechanical Engineers, Fourth International Conference, Turbocharging and Turbochargers* pp. 123–132.
- CAPOBIANCO, M. & GAMBAROTTA, A. 1992 Variable geometry and waste-gated automotive turbochargers: Measurements and comparision of turbine performance. *Transactions of ASME: Journal of Engineering for Gas Turbines and Power* **114**, 553–560.
- CAPOBIANCO, M. & GAMBAROTTA, A. 1993 Performance of a twin-entry automotive

- turbocharger turbine. *ASME, 93- ICE-2. Energy-Sources Technology Conference & Exhibition*. pp. 1–10.
- CAPOBIANCO, M. & MARELLI, S. 2005 Transient performance of automotive turbochargers: Test facility and preliminary experimental analysis. *SAE 2005-24-066, ICE 2005, 7th International Conference on Engines for Automobile* .
- CARPINLIOGLU, M. & GUNDOGDU, M. 2001 A critical review on pulsatile flow studies directing towards future research topics. *Flow measurements and Instrumentations* **12**, 165–174.
- CD-ADAPCO 2005 *Methodology manual*. STAR-CD Version 3.26.
- CELIK, I. B. 2005 Procedure for estimation and reporting of discretization error in cfd applications. *Internal report, Mechanical and Aerospace Engineering Department, West Virginia University, Morgantown Wv, USA, is-mail.celik@mail.wvu.edu* .
- CHAPPLE, P., FLYNN, P. F. & MULLOY, J. 1980 Aerodynamical design of fixed and variable geometry nozzleless turbine casings. *Transactions of the ASME Journal Eng for Power* **102**, 141–147.
- CHEN, H., BAINES, N. C. & ABIDAT, M. 1997 Exit traverse study of mixed-flow turbines with inlet incidence variation. *Proceedings of the Institute of Mechanical Engineers* **211 Part A**, 461–475.
- DALE, A. & WATSON, N. 1986 Vaneless radial turbocharger turbine performance. *ImechE Conference Transactions; "Turbochargers and Turbocharging"*, London pp. 65–76.
- DAMBACH, R. & HODSON, H. 2001 Tip leakage flow in a radial inflow turbine with varying gap height. *Journal of Propulsion and Power* **17**, 644–650.
- DEC, J. E. & KELLER, J. O. 1989 Pulse combustor tail-pipe heat-transfer dependence on frequency, amplitude and mean flow rate. *Combustion and flame* pp. 359–374.
- DEC, J. E., KELLER, J. O. & HONGO, I. 1991 Time-resolved velocities and turbulence in oscillating flow of a pulse combustor tail pipe. *Combustion and flame* **83**, 271–292.
- DORAN, W. J., SPENCE, S. W. T. & ARTT, D. W. 2001 Experimental performance evaluation of a 99.0 mm radial inflow nozzled turbine with varying shroud profiles. *Proceedings of the Institute of Mechanical Engineers: Journal of Power and Energy* **215**, 267–280.
- FILIPPI, Z., WANG, Y. & ADDANIS, D. 2001 Effect of variable geometry turbine (vgt) on diesel engine and vehicle system transient respons. *SAE 2001 World Congress, Detroit, Michigan SAE 2001-01-1247*, 1–19.
- FLAXINGTON, A. & SWAIN, E. 1999 Turbocharger aerodynamic design. *Proceedings of the Institute of Mechanical Engineers Vol 213 Part C*, 43–57.
- FUKAYA, M., WATANABE, M. & UDAGAWA, T. 2000 Compressible turbulent flow analysis on variable nozzle vanes and spacer in turbocharger turbine. *SAE 2000 World Congress, Detroit, Michigan SAE 2000-01-0526*.
- FUTRAL, S. M. & HOLESKI, D. E. 1970 Experimental results of varying the blade-shroud clearance in a 6.02-inch radial-inflow turbine. *Tech. Rep.*. NASA TN D-5513.

- GERMANO, M., PIOMELLI, U., MOIN, P. & CABOT, W. 1991 A dynamic subgrid-scale eddy viscosity model. *Physics of Fluids* **3**, 1760–1764.
- GHOSAL, S., LUND, T., MOIN, P. & AKSELVOLL, K. 1995 A dynamic localization model for large-eddy simulations of turbulent flows. *Journal of Fluid Mechanics* **286**, 229–255.
- HABIB, M., ATTYA, A., SAID, S., EID, A. & ALY, A. 2004 Heat transfer characteristics and nusselt number correlation of turbulent pulsating pipe air flows. *Heat and Mass Transfer* **40**, 307–318.
- HAMAKIOTES, C. & BERGER, S. 1988 Fully developed pulsatile flow in a curved pipe. *Journal of Fluid Mechanics* **195**, 22–55.
- ISSA, R. 1986 Solution of the implicit discretised fluid flow equations by operator-splitting. *Journal of Computational Physics* **62**, 40–65.
- ISSA, R., AHMADI BEFRUI, B., BESHAY, K. & GOSMAN, A. 1991 Solution of the implicitly discretised reacting flow equations by operator-splitting. *Journal of Computational Physics* **93**, 388–410.
- ISSA, R., GOSMAN, A. & WATKINS, A. 1986 The computation of compressible and incompressible recirculation flows by a non-iterative implicit scheme. *Journal of Computational Physics* **62**, 66–82.
- JEONG, J. & HUSSAIN, F. 1995 On the identification of a vortex. *Journal of Fluid Mechanics* **285**, 69–94.
- JOHANSSON, A. V. & ALFREDSSON, P. H. 1988 *Experimental methods in fluid mechanics*. Dept. of Mechanics, Royal Institute of Technology, Stockholm.
- KARAMANIS, N., MARTINEZ-BOTAS, R. & SU, C. 2001 Mixed flow turbines: Inlet and exit flow under steady and pulsating conditions. *ASME Journal of Turbomachinery* **123**, 359–371.
- KLEIN, M., SADIKI, A. & JANICKA, J. 2003 A digital filter based generation of inflow data for spatially developing direct numerical or large eddy simulations. *Journal of Computational Physics* **186**, 652–665.
- LAM, J. K. W., ROBERTS, Q. D. H. & MCDONNELL, G. T. 2002 Flow modelling of a turbocharger turbine under pulsating flow. *ImechE Conference Transactions from 7th International Conference on Turbochargers and Turbocharging, 14-15 May London UK* pp. 181–196.
- LYNE, W. 1970 Unsteady viscous flow in a curved pipe. *Journal of Fluid Mechanics* **45**, 13–31.
- MATTINGLY, G. & YEH, T. 1991 Effects of pipe elbows and tube bundles on selected types of flowmeters. *Flow Meas. Instrum* **2**, 4–13.
- MOUSTAPHA, H., ZELESKY, M., BAINES, N. & JAPISKE, D. 2003 *Axial and radial Turbines*. Concepts NREC.
- NAJAFI, A., SAIDI, M.S. AND SADEGHIPOUR, M. & SOUHAR, M. 2005 Numerical analysis of turbulent swirling decay pipe flow. *International Communications in Heat and Mass Transfer* **32**, 627–638.
- PALFREYMAN, D. & MARTINEZ-BOTAS, R. 2005 The pulsating flow field in a mixed flow turbocharger turbine: An experimental and computational study. *ASME, Journal of Turbomachinery* **127**, 144–155.

- PALFREYMAN, D., MARTINEZ-BOTAS, R. F. & KARAMANIS, N. 2002 Computational and experimental investigation of the aerodynamics of turbocharger mixed-flow turbines. *ImechE Conference Transactions from 7th International Conference on Turbochargers and Turbocharging, 14-15 May London UK* pp. 45–59.
- PESIRIDIS, A. & MARTINEZ-BOTAS, R. 2006 Active control turbocharger for automotive application: An experimental evaluation. *ImechE Conference Transactions from 8th International Conference on Turbochargers and Turbocharging* pp. 223–234.
- RAJOO, S. & MARTINEZ-BOTAS, R. 2007 Improving energy extraction from pulsating flow by active control of a turbocharger turbine. *SAE 2007-01-1557*.
- RAMAPRIAN, B. R. & TU, S. W. 1983 Fully developed periodic turbulent pipe flow. part 2. the detailed structure of the flow. *J. of Fluid Mechanics* **137**, 59–81.
- ROGO, C., HAJEK, T. & CHEN, A. 1986 Variable stator radial turbine. *Tech. Rep.* NASA CR-174663.
- RUTTEN, F., SCHRODER, W. & MEINKE, M. 2005 Large eddy simulation of low frequency oscillations of the dean vortices in turbulent pipe bend flows. *Physics of Fluids* **17**.
- SPENCE, S., ROSBOROUGH, R., ARTT, D. & MCCULLOUGH, G. 2007 A direct performance comparison of vaned and vaneless stators of radial turbines. *Journal of Turbomachinery* **129**, 53–61.
- SPENCE, S. W. T. & ARTT, D. W. 1998 An experimental assessment of incidence losses in a radial inflow turbine rotor. *Proceedings of the Institute of Mechanical Engineers. Part A: Journal of Power and Energy* **212**, 43–53.
- STEENBERGEN, W. & VOSKAMP, J. 1998 The rate of decay of swirl in turbulent pipe flow. *Flow Measurements and Instrumentations* **9**, 67–78.
- SUDO, K., SUMIDA, H. & HIBARA, H. 2000 Experimental investigation on turbulent flow through a circular-sectioned 180° bend. *Experiments in Fluids* **28**, 51–57.
- SUDO, K., SUMIDA, H. & HIBARA, H. 1998 Experimental investigation on turbulent flow through a circular-sectioned 90° bend. *Experiments in Fluids* **25**, 42–49.
- WALLACE, F., ADGEY, J. & BLAIR, G. 1969 Performance of inward radial flow turbines under non-steady flow conditions. *Proc Instn Mech Engrs* **184**, 183–195.
- WALLACE, F. & BLAIR, G. 1965 The pulsating-flow performance of inward radial flow turbines. *American Society of Mechanical Engineers Publ.* **65-GTP-21**, 1–20.
- WANG, X. & ZHANG, N. 2005 Numerical analysis of heat transfer in pulsating turbulent flow in a pipe. *International Journal of Heat and Mass Transfer* **68**, 3957–3970.
- WINTERBONE, D. E., NIKPOUR, B. & ALEXANDER, G. I. 1990 Measurements of the performance of a radial inflow turbine in conditional steady and unsteady flow. *ImechE Conference Transactions, 4th International Conference: Turbocharging and turbocharging* **C405/015**, 153–160.
- WINTERBONE, D. E., NIKPOUR, B. & FROST, H. 1991 A contribution to the

- understanding of turbocharger turbine performance in pulsating flow. *International Conference on Internal Combustion Research, Paper no C433/011. Inst. of Mech. Engrs.* pp. 19–28.
- YEO, J. H. & BAINES, N. C. 1990 Pulsating flow and behaviour in a twin-entry vaneless radial-inflow turbine. *ImechE Conference Transactions, 4th International Conference: Turbocharging and turbocharging.* **C405/004**, 113–122.